# ICOS signaling limits regulatory T cell accumulation and function in visceral adipose tissue

Kristen L. Mittelsteadt[1,2] and Daniel J. Campbell[1,2,3*]

[1]Immunology Research Program, Benaroya Research Institute, Seattle, WA 98101
[2]Molecular and Cellular Biology Program, University of Washington, Seattle, WA 98195
[3]Department of Immunology, University of Washington, Seattle, WA 98195

[*]Corresponding Author: Daniel J. Campbell, Benaroya Research Institute, 1201 Ninth Avenue, Seattle, WA 98101. Email address: campbell@benaroyaresearch.org

Running Title: ICOS signaling in VAT-$T_R$

**Abstract**
A unique population of Foxp3$^+$ regulatory T cells ($T_R$) resides in visceral adipose tissue (VAT) that regulates adipose inflammation and helps preserve insulin sensitivity. The costimulatory molecule ICOS is highly expressed on effector (e)$T_R$ that migrate to nonlymphoid tissues, and contributes to their maintenance and function in models of autoimmunity. In this study, we report an unexpected cell-intrinsic role for ICOS expression and downstream PI3K signaling in limiting the abundance, VAT-associated phenotype, and function of $T_R$ specifically in VAT. *Icos*$^{-/-}$ mice and mice expressing a knock-in form of ICOS that cannot activate PI3K had increased VAT-$T_R$ abundance and elevated expression of canonical VAT-$T_R$ markers. Loss of ICOS signaling facilitated enhanced accumulation of $T_R$ to VAT associated with elevated CCR3 expression, and resulted in reduced adipose inflammation and heightened insulin sensitivity in the context of high-fat diet. Thus, we have uncovered a new and surprising molecular pathway that regulates VAT-$T_R$ accumulation and function.

## Introduction

$CD4^+Foxp3^+$ regulatory T cells ($T_R$) are critical for the development and maintenance of immune tolerance, the inhibition of immune responses to innocuous environmental antigens, and the resolution of ongoing inflammation after infection (*1–3*). More recent work highlights additional roles for specialized subsets of tissue-specific $T_R$ in tissue repair and homeostasis. For example, $Areg^+$ $T_R$ expand in skeletal muscle and the lungs in response to injury and are required for proper tissue repair (*4*, *5*), whereas $T_R$ within hair follicles and skin are essential for hair generation and keeping profibrotic processes in check, respectively (*6*, *7*). A transcriptionally unique population of $T_R$ are found in the visceral adipose tissue (VAT) of both mice and humans, and these $T_R$ regulate adipose inflammation and preserve metabolic homeostasis as demonstrated by loss- and gain-of-function experiments (*8–11*). For example, $T_R$ ablation in diphtheria toxin-treated *Foxp3*$^{DTR}$ mice results in increased inflammatory mediators in VAT and reduced insulin sensitivity, whereas augmentation of $T_R$ by administration of IL-2 immune complexes or IL-33 results in improved metabolic readouts in mice on high-fat diet (HFD) (*8*, *12*, *13*).

Given that $T_R$ modulate diverse responses in different anatomical and inflammatory settings, it is not surprising that they exhibit considerable phenotypic and functional heterogeneity. Expression of CD62L and CD44 broadly divides $T_R$ into distinct subsets that are enriched in lymphoid and nonlymphoid tissues (*14*, *15*). We term these populations central $T_R$ ($cT_R$) and effector $T_R$ ($eT_R$), respectively. Differential activation of PI3K, unique epigenetic landscapes, and distinct transcriptional programs drive functional diversification of $T_R$, and selective expression of chemokine receptors and cell adhesion molecules give subsets of $T_R$ access to specific tissues (*16–18*). The proper distribution and function of $T_R$ across tissues is crucial for maintaining immune tolerance and tissue homeostasis (*19*, *20*). Hence, understanding the signals that control the development, maintenance, and function of tissue-specific $T_R$ is vital to fully harnessing their therapeutic potential.

$T_R$ occupancy in lymphoid versus nonlymphoid tissues is met with unique homeostatic maintenance requirements. Generally, IL-2 signaling maintains $cT_R$ within T cell zones of secondary lymphoid tissues by driving pro-survival signals, whereas maintenance of $eT_R$ in nonlymphoid tissues can be IL-2 independent and instead relies on TCR and costimulatory molecule engagement (*14*, *21, 22*). ICOS is expressed on highly suppressive $T_R$ and can control $T_R$ abundance by inhibiting apoptosis and stimulating proliferation (*23*, *24*). ICOS can also impact $T_R$ function. $T_R$ production of the immunosuppressive cytokine IL-10 is essential for control of local immune responses, and is primarily expressed by Blimp-$1^+ICOS^+$ $eT_R$ (*25*). ICOS costimulation *in vitro* super-induces IL-10 expression (*26*, *27*), and this depends on its ability to activate phosphoinositide 3-kinase (PI3K) (*28*, *29*). Although mice deficient in ICOS or ICOS ligand do not develop spontaneous inflammatory or autoimmune disease, genetic or antibody-mediated blockade of ICOS signaling promotes inflammatory immune responses in mouse models of autoimmunity and infection as a result of reduced $T_R$ abundance and/or IL-10 production (*23*, *30–36*).

ICOS potently activates PI3K and downstream AKT due to the presence of a unique YMFM motif in its cytoplasmic tail (*26, 37*). AKT can act on several different substrates, including the transcription factor Foxo1, to modulate transcription of genes

involved in proliferation, survival, metabolic reprogramming, and migration/tissue tropism (*38*). Indeed, inactivation of Foxo1 by AKT is essential for the differentiation of $eT_R$ and their migration to nonlymphoid tissues (*16*). Thus, engagement of ICOS may facilitate the development and/or maintenance of $eT_R$ via PI3K-dependent signaling pathways.

Accumulation of $T_R$ in VAT is dependent on several signals. Local TCR:MHCII interactions are likely important, as VAT-$T_R$ consist of clonally expanded populations, suggesting recognition of one or more adipose tissue antigens (*8*, *39*). A fraction of VAT-$T_R$ express the IL-33 receptor, ST2. Indeed, mice lacking expression of IL-33 or ST2 are deficient in VAT-$T_R$, whereas injection of exogenous IL-33 results in increased VAT-$T_R$ abundance with little impact on lymphoid $T_R$ (*12*, *13*). Recent work assessing WT:*Ccr2*$^{-/-}$ mixed bone marrow chimeric mice also identified a cell-intrinsic role for CCR2 in the ability of donor $T_R$ to repopulate VAT (*40*). Finally, $T_R$ expression of PPARγ, the master regulator of adipocyte differentiation, supports VAT-$T_R$ phenotype and accumulation and drives expression of factors important for lipid metabolism (*41*, *42*). However, despite having an $eT_R$ phenotype, the role of costimulatory molecule signaling in VAT-$T_R$ is poorly understood.

In this study, we demonstrate an unexpected role for cell-intrinsic ICOS-dependent PI3K signaling in restricting VAT-$T_R$ accumulation and activated phenotype. Moreover, we implicate the CCL11/24-CCR3 axis in driving recruitment of $T_R$ to VAT, which is enhanced in the absence of ICOS signaling. These surprising findings challenge the current model regarding signals that support diverse $T_R$ subsets, and highlights the cell- and tissue-specific effects of ICOS expression and signaling on $T_R$ development, accumulation, and function.

## Results

### *Mice lacking ICOS signaling have reduced $T_R$ in lymphoid tissues and altered expression of PI3K targets*

To determine how ICOS signaling impacts $T_R$ abundance in different tissues, we crossed *Foxp3*$^{mRFP}$ mice to *Icos*$^{-/-}$ (KO) mice and to *Icos*$^{Y181F}$ (YF) mice, which carry a tyrosine-to-phenylalanine knock-in mutation in the YMFM motif in the cytoplasmic tail of ICOS, thereby specifically abolishing ICOS-mediated PI3K activation (*43*). Thus we had WT, YF, and KO mice whose $T_R$ expressed monomeric red fluorescent protein (RFP) under control of the *Foxp3* locus, faithfully marking $T_R$ without the need for intracellular Foxp3 staining (*44*). In line with published data, we found a ~30% reduction in the frequency and number of $T_R$ in the spleens of KO compared to WT mice (*24*, *34*) **[Fig. 1A]**. This was even more pronounced in older animals, as $T_R$ accumulate with age (*45*) **[Fig. 1B]**. Despite normal ICOS expression on the cell surface **[Supp. Fig. 1A]** and intact MAPK signaling (*43*), we saw a similar reduction in splenic $T_R$ abundance in YF mice, indicating that activation of PI3K signaling is the critical pathway by which ICOS regulates $T_R$ abundance **[Fig. 1A, 1B]**. ICOS is expressed on both $cT_R$ and $eT_R$, however its expression is upregulated on $eT_R$ **[Supp. Fig. 1B]**. The loss of $T_R$ we observed in YF and KO spleens was associated with a disproportionate reduction in the frequency and number of $eT_R$, whereas the number of $cT_R$ was unchanged, consistent with results from our lab using *in vivo* antibody blockade of ICOS signaling (*14*) **[Fig. 1C]**. Loss of $T_R$ was also observed in the peripheral lymph nodes of YF and KO mice,

indicating that ICOS signaling is important for $eT_R$ maintenance in multiple secondary lymphoid organs **[Supp. Fig. 1C]**. Both YF and KO $T_R$ in the spleen had altered expression of targets controlled by PI3K signaling, including elevated expression of the lymphoid homing molecules CD62L and CCR7 which are downregulated upon PI3K activation via phosphorylation and sequestration of Foxo1 (*46*) **[Fig. 1D]**. When examined directly *ex vivo*, YF and KO splenic $T_R$ also exhibited reduced phosphorylation of the mTORC1 target, ribosomal protein S6, consistent with diminished activation of PI3K **[Fig. 1E]**. This further indicates that absence of ICOS-mediated PI3K activation drives the altered lymphoid $T_R$ frequency and phenotype we see in YF and KO mice.

*$T_R$ are enriched in VAT in the absence of ICOS signaling*

As $eT_R$ are highly enriched in nonlymphoid sites (*14*, *47*), we next assessed whether maintenance of $T_R$ in peripheral tissues was diminished in YF and KO mice. Using intravascular labeling to identify tissue-localized $T_R$ (*48*), we observed a reduction in the frequency and number of $T_R$ in the skin and decrease in the absolute number of $T_R$ in the lungs of YF and KO mice [**Fig. 2A, 2B]**. However, $T_R$ frequency and total number were actually elevated in the VAT of both strains **[Fig. 2C]**. This was specific to VAT, as frequency and total number of $T_R$ in subcutaneous adipose tissue (SQAT) remained similar between genotypes **[Supp. Fig. 2A]**. The increased abundance of VAT-$T_R$ in YF and KO mice was present in both males and females, although the frequency and number of VAT-$T_R$ was significantly reduced in females **[Fig. 2D, 2E]**. Consistent with previous studies, we observed age-dependent accumulation of VAT-$T_R$ across all three genotypes (*8*), but despite considerable mouse-to-mouse variability, VAT-$T_R$ remained elevated in YF and KO mice across all age groups analyzed **[Fig. 2F].**

We utilized male mice for the remainder of our studies as we found female mice harbor ~4-5-fold fewer $T_R$/gram VAT than age-matched males, and female mice are protected from the development of diet-induced metabolic syndrome (*40*, *49*, *50*). The frequency of VAT-$T_R$ expressing KLRG1 and CD69 was significantly elevated in YF and KO mice compared to WT controls **[Fig. 3A]**. This is in contrast to what we found in the spleen, where a reduced frequency of YF and KO $T_R$ expressed CD69, and very few $T_R$ expressed KLRG1 **[Supp. Fig. 3A]**. We assessed VAT-$T_R$ Foxp3 and CD44 expression, and found no difference in the absence of ICOS **[Supp. Fig. 3B]**. We did however observe a modest increase in the expression of CTLA-4 and a slight reduction in the frequency of $CD25^+$ $T_R$ in YF and KO VAT **[Fig. 3A]**. Therefore, $T_R$ in the VAT of YF and KO mice are enriched in expression of markers indicative of an $eT_R$ and VAT-$T_R$ phenotype (*8*, *14*).

In addition to prototypical $eT_R$ markers, a fraction of VAT-$T_R$ express the IL-33 receptor, ST2 (*12*, *39*). Signaling downstream of ST2 is required for the establishment and maintenance of VAT-$T_R$, and expansion of VAT-$T_R$ through administration of IL-33 can reduce VAT inflammation and improve metabolic indices in models of diet-induced obesity (*12*, *13*, *39*). In addition to ST2-expressing $T_R$, we found a substantial population of $CXCR3^+$ $T_R$ in the VAT of lean mice, confirming previously reported findings **[Fig. 3B]** (*51*). Although there were no significant differences in the frequency of WT, YF, or KO VAT-$T_R$ singly-expressing ST2 or CXCR3, we found a unique population of double-

expressing ST2$^+$CXCR3$^+$ $T_R$ in YF and KO VAT which resembled canonical VAT-$T_R$ in their expression of KLRG1 and CD69 **[Fig. 3B, 3C]**.

ICOS signaling is implicated in IL-10 production both *in vitro* and *in vivo* (*23*, *26*, *27*, *30–36*). Surprisingly, compared to VAT-$T_R$ from WT mice, a substantially higher frequency of YF and KO VAT-$T_R$ were poised to produce IL-10 upon *ex vivo* stimulation with PMA/I, with no appreciable differences in IL-10 expression by splenic $T_R$ **[Fig. 3D]**. Thus, absence of ICOS-dependent PI3K signaling supports both the accumulation and suppressive phenotype of $T_R$ in VAT.

*Baseline adipose inflammation is reduced in YF and KO mice*

$T_R$ regulate inflammatory responses in VAT, so we next assessed whether the loss of ICOS signaling resulted in changes in VAT inflammation. VAT inflammation is modulated through a balance of different immune cells. $T_R$, eosinophils, alternatively activated anti-inflammatory adipose tissue macrophages (ATM), and group-2 innate lymphoid cells (ILC2) maintain a type-2 immune environment that supports metabolic homeostasis in lean animals. Inflammation however drives recruitment of neutrophils and cytotoxic T cells, differentiation of inflammatory ATM, and production of pro-inflammatory cytokines like TNFα (*52*, *53*). Although there was no difference in mouse weights between WT, YF, and KO mouse across different ages, we did observe a trend toward increased VAT weight in YF mice, and a significant increase in KO mice **[Fig. 4A]**. By histology, we did not observe any overt morphological differences in VAT from WT, YF, and KO mice, including no observable differences in adipocyte size **[Supp. Fig. 4A].** This increase in VAT weight however did correlate with a modest increase in the total number of CD4$^+$ $T_{eff}$ per gram of tissue **[Fig. 4B]**. Despite this increase in VAT-$T_{eff}$ number, there was a substantially lower frequency of YF and KO VAT-$T_{eff}$ expressing features of inflammatory $T_H1$ cells, including CXCR3, IFNγ, and TNFα **[Fig. 4C]**. Rather, ST2-expressing $T_{eff}$ were enriched in YF and KO VAT **[Fig. 4C]**. Similar to VAT-$T_R$, YF and KO VAT-$T_{eff}$ were superior at producing IL-10 upon stimulation, suggesting that absence of ICOS signaling in effector cells supports a self-regulatory function **[Fig. 4C]**. IL-33 signaling induces production of $T_H2$ cytokines (*54*), which maintain ATM in an anti-inflammatory state. While we didn't find any significant changes in ATM or ILC2 populations **[Supp. Fig. 4B, 4C]**, we did note an increased frequency of eosinophils in YF and KO VAT **[Fig. 4D]**, which produce IL-4 to maintain anti-inflammatory ATM (*52*, *55*). Overall, global loss of ICOS expression and signaling impacts $T_R$ along with other adipose-resident immune cells to maintain an anti-inflammatory state in VAT.

*YF and KO mice are protected from high-fat diet-induced insulin resistance, correlating with maintenance of VAT-$T_R$*

Given the abundance and suppressive phenotype of $T_R$ and other anti-inflammatory immune cells in VAT in the absence of ICOS signaling, we wondered if this would render YF and KO mice more resistant to developing HFD-induced inflammation and metabolic changes. Mice placed on an 18-week HFD steadily gained body mass, with a modest reduction in weight gained by KO mice compared to WT **[Fig. 5A]**. After 18 weeks on HFD, YF and KO mice sustained elevated $T_R$ frequencies in VAT compared to WT mice, with an increased fraction of cells expressing the canonical

VAT-$T_R$ markers ST2 and KLRG1, and a smaller proportion of $T_R$ expressing CXCR3 **[Fig. 5B, 5C]**. Additionally, YF and KO mice placed on HFD retained a greater frequency of eosinophils and $T_{eff}$ skewed toward a type-2, ST2-expressing phenotype **[Fig. 5D, 5E]**. Fasting blood glucose levels (BGL) were similar among genotypes after 18-weeks, and WT, YF, and KO mice were able to clear glucose to the same extent, as measured by glucose tolerance test (GTT) **[Fig. 5F]**. However, in an insulin tolerance test (ITT), YF and KO mice demonstrated improved insulin sensitivity compared to WT mice **[Fig. 5G]**. Thus, loss of ICOS supports $T_R$ and other anti-inflammatory cells in VAT during HFD, and this has functional consequences in maintaining metabolic homeostasis.

*Absence of ICOS supports the accumulation and phenotype of VAT-$T_R$ in a cell-intrinsic manner*

ICOS signaling supports a wide array of cellular processes in the context of adaptive immunity, including induction and localization of T follicular helper cells, T-dependent antibody production, and $CD4^+$ $T_{eff}$ polarization and function (*56*). To assess which of the T cell phenotypes we observed in intact YF and KO mice were the result of intrinsic ICOS expression and signaling, we generated mixed bone marrow chimeras using congenically marked $CD45.1^+$ WT and $CD45.2^+$ WT, YF, or KO donors **[Fig. 6A]**. Body and adipose depot weights were similar between groups of chimeric mice **[Supp. Fig. 5A]**. Consistent with the increased abundance of VAT-$T_R$ we observed at baseline in intact YF and KO mice, both $CD45.2^+$ YF and KO $T_R$ displayed a competitive advantage compared to $CD45.1^+$ WT $T_R$ in repopulating VAT in our chimeric mice. While WT:WT chimeras reconstituted VAT-$T_R$ at a ~1:1 ratio, YF and KO $T_R$ exhibited a significantly higher reconstitution ratio of ~5.5:1 **[Fig. 6B]**. In addition to supporting VAT-$T_R$ abundance, absence of cell-intrinsic ICOS signaling also promoted a canonical VAT-$T_R$ phenotype. Within the same chimeras, a higher frequency of YF and KO VAT-$T_R$ expressed CD69 and ST2 **[Fig. 6C]**. Aligned with data from intact mice, more YF and KO VAT-$T_R$ within chimeras were double-expressers of CXCR3 and ST2 **[Fig. 6C]**. Functionally, a larger proportion of YF and KO VAT-$T_R$ were poised to produce IL-10 after *ex vivo* stimulation **[Fig. 6C]**. Mixed bone marrow chimeras retain a population of radioresistant host $T_R$, which proliferate to replenish a portion of the available niche after irradiation (*57*), and this is particularly evident in many nonlymphoid tissues. Remarkably, in addition to preferentially reconstituting VAT compared to WT donor $T_R$, YF and KO VAT-$T_R$ were able to outcompete endogenous WT VAT-$T_R$ as well, nearly replacing the entire $T_R$ compartment in some chimeras **[Fig. 6D]**.

Contrary to our findings in VAT, YF and KO $T_R$ were at a selective disadvantage in the skin, spleen, and large intestine, with no difference in reconstitution in the lungs **[Fig. 6E, Supp. Fig. 5B]**. $T_R$ found in SQAT are phenotypically distinct from VAT-$T_R$ and do not appear to accumulate with age (*8*, *51*). However, unlike in intact mice, we did note that YF and KO donor $T_R$ displayed a competitive advantage in repopulating SQAT in chimeric mice at a ratio of ~3:1 **[Fig. 6E]**. This could be due to low level inflammation following irradiation of the recipient mice that drives reconstitution of the SQAT niche with $T_R$ exhibiting a more VAT-$T_R$ phenotype.

Although $CD8^+$ T cells and ILC2s of either genotype were similarly represented **[Supp. Fig. 5C]**, we did find that YF and KO $T_{eff}$ were modestly, but significantly,

enriched in VAT, at a ~2:1 ratio compared to WT $T_{eff}$ with no difference in reconstitution of other tissues **[Fig. 6F]**. A higher frequency of YF and KO VAT-$T_{eff}$ were $ST2^+$ within the same chimeras, with a reduction in CXCR3-expressing $T_{eff}$ **[Fig. 6G]**. Functionally, YF and KO VAT-$T_{eff}$ were comprised of fewer IFNγ$^+$ and TNFα$^+$ and more IL-10$^+$ cells when stimulated *ex vivo* **[Fig. 6G]**, indicating that in addition to driving increased $T_R$ abundance, the absence of ICOS signaling also promotes a regulatory phenotype in VAT-$T_{eff}$. Taken together, loss of ICOS signaling supports VAT-$T_R$, and to a lesser extent, $T_{eff}$ accumulation and phenotype through cell-intrinsic mechanisms.

*ICOS signaling impacts expression of homing receptors in $T_R$ that allow access to VAT*

The increased abundance of VAT-$T_R$ from YF and KO mice could be the result of three non-mutually exclusive processes: increased proliferation; increased survival; or increased migration to the VAT. The proliferation marker Ki67 was generally expressed by ~10-20% of VAT-$T_R$, and we found no significant difference in the frequency of Ki67$^+$ VAT-$T_R$ between WT, YF, and KO mice **[Fig. 7A]**. Similarly, WT, YF, and KO VAT-$T_R$ expressed similar levels of the pro-survival protein Bcl2 **[Fig. 7B]**, and together these results suggest that differences in cellular turnover are not responsible for the accumulation of YF and KO $T_R$ seen in VAT.

In both intact and mixed bone marrow chimeric mice, YF and KO splenic $T_R$ contained a small but significantly increased population of $ST2^+$ $T_R$ **[Fig. 8A, 8B]**, a subset of $T_R$ that is both transcriptionally and epigenetically poised to take up residence in peripheral tissues (*17*, *58*). Given this, we hypothesized that superior migration and accumulation could account for the increased frequency of VAT-$T_R$ in YF and KO mice. Although CCR2 facilitates recruitment of $T_R$ to VAT (*40*), we detected no difference in CCR2 expression among genotypes, and a modest decrease in $CCR2^+$ $T_R$ in KO spleens **[Supp. Fig. 6A]**, arguing against enhanced CCR2-mediated recruitment of YF and KO $T_R$ to VAT.

Previous studies identified both an open chromatin landscape around the *Ccr3* locus as well as high transcript levels in VAT-$T_R$ (*41*, *51*). The frequency of CCR3-expressing splenic $T_R$ was slightly elevated in both young (≤8 weeks) and older (>8 weeks) YF and KO mice **[Supp. Fig. 6B]**, indicating the presence of a $T_R$ population primed for both potential early seeding and continuous repopulation of peripheral tissues. In line with this, YF and KO VAT contained more $CCR3^+$ $T_R$ compared to WT mice and this population increased with age **[Fig. 8C]**. In mixed bone marrow chimeras, a significantly greater frequency of YF and KO donor $T_R$ were $CCR3^+$ in spleen and VAT **[Supp. Fig. 6C]**. Additionally, YF and KO VAT contained a unique population of $T_R$ that expressed CCR3 alone, while WT VAT-$T_R$ expressing CCR3 were also positive for CCR2 **[Fig. 8D]**. CCR3 expression was unique to VAT-$T_R$, unlike CCR2, which we found to be also highly expressed on VAT-$T_{eff}$ **[Fig. 8C, Supp. Fig. 6A]**. Additionally, the accumulation of $CCR3^+$ $T_R$ was unique to VAT, as we detected very little CCR3 expression in skin, lungs, and large intestine $T_R$ and no differences across genotypes **[Supp. Fig. 6D, 6E].** Within the VAT, we detected substantial expression of the CCR3 ligands *Ccl11* and *Ccl24* with no differences detected either by age or genotype and little expression of *Ccl5*, *Ccl7*, and *Ccl26* **[Fig. 8E]**.

We next assessed whether ICOS signaling could directly impact expression of CCR3 on $T_R$. WT, YF, and KO VAT-$CD4^+$ cells were cultured with αCD3/αCD28 and IL-

2 in the presence or absence of an agonistic αICOS antibody **[Fig. 8F]**. After 48 hr in culture, $T_R$ frequency remained unchanged in both groups. However, the frequency of $CCR3^+$ $T_R$ in WT cultures significantly decreased after 2 days with addition of an ICOS agonist, whereas no changes were observed in YF or KO cultures, indicating that ICOS-dependent PI3K signaling can directly antagonizing CCR3 expression in $T_R$ **[Fig. 8F]**.

To address the impact of CCR3 signaling on continuous $T_R$ seeding of VAT *in vivo*, we administered blocking antibodies to the CCR3 ligands CCL11 and CCL24 to 8-10 week old WT and YF mice. Blockade of CCL11/24 for ~2 weeks resulted in a modest although not statistically significant decrease in the frequency of VAT-$T_R$ specifically in YF mice, with no differences in $T_R$ abundance in spleen or lungs between treated and untreated mice **[Fig. 8G]**. We additionally noted a slight reduction in VAT-eosinophils in YF mice treated with αCCL11/24 **[Supp. Fig. 6F]**. Together, these results suggest a potential mechanism by which loss of ICOS-dependent PI3K signaling can drive increased recruitment of $T_R$ to VAT by CCR3-CCL11/24 interactions.

## Discussion

We have identified surprising tissue-specific effects of ICOS signaling on $T_R$ abundance and phenotype. Although there was a significant loss of $CD44^+$ $eT_R$ in the spleen, pLN, skin, and lungs of YF and KO mice compared to WT, we unexpectedly observed a substantial increase in $T_R$ abundance in VAT. $T_R$ frequency and phenotype were similar in YF and KO mice, including comparably altered readouts of PI3K signaling, suggesting that ICOS primarily impacts $T_R$ abundance and homeostasis via PI3K-dependent mechanisms.

In addition to supporting VAT-$T_R$ abundance, loss of ICOS signaling promoted a highly suppressive VAT-$T_R$ phenotype, including an increased proportion of $T_R$ expressing KLRG1, CD69 and IL-10. *In vitro*, addition of ICOS stimulation augments IL-10 production in $CD4^+$ T cells while loss of ICOS signaling *in vivo* results in reduced $T_R$ abundance and IL-10 expression in models of autoimmunity, allergy, and infection (*23*, *26*, *27*, *31*, *32*, *34*, *35*). Although ICOS expression is associated with IL-10-producing $T_R$, ICOS signaling does not appear to be intrinsically required for IL-10 production. $CD4^+$ T cells from KO mice are capable of producing WT levels of IL-10 *in vitro*, and interestingly, appear to produce more IL-10 than WT counterparts under $T_H2$-polarizing conditions (*33*). Furthermore, recent studies assessing $T_R$ in the brain during chronic *Toxoplasma gondii* infection and lamina propria $T_R$ at baseline report no changes in IL-10 production in the presence or absence of ICOS signaling (*34*, *59*). Therefore, the reduction in IL-$10^+$ $T_R$ with ICOS blockade observed in specific *in vivo* models is likely due to insufficient activation or access to specific environmental cues within tissues rather than an inherent requirement for ICOS signaling to drive IL-10 production.

VAT is a complex tissue, consisting of triglyceride-containing adipocytes and a variety of immune cells which function to maintain metabolic homeostasis. In YF and KO mice, other immune cells in addition to $T_R$ showed evidence of an anti-inflammatory phenotype. Although ATM and VAT-ILC2 abundance was similar across genotypes at baseline, eosinophil frequency was significantly elevated in YF and KO VAT. In YF and KO mice, VAT-$T_{eff}$ were skewed toward a $T_H2$ phenotype in a cell-intrinsic manner, with an increased frequency of ST2-expressing and IL-10-producing cells. Therefore, in addition to promoting an anti-inflammatory state by sustaining VAT-$T_R$, global loss of

ICOS signaling supports the abundance and phenotype of other anti-inflammatory adipose-resident immune cells. These combined changes in cellular composition in VAT in the absence of ICOS signaling were maintained in the setting of long-term HFD, and rendered YF and KO mice more resistant to HFD-induced loss of insulin sensitivity.

YF and KO donor $T_R$ preferentially repopulated VAT in mixed bone marrow chimeras, and were able to outcompete both donor and endogenous WT $T_R$. ST2 is expressed on a large fraction of VAT-$T_R$ (*12*), and although we didn't note any differences in the frequency of ST2-expressing VAT-$T_R$ in intact mice, YF and KO VAT-$T_R$ in mixed bone marrow chimeras were comprised of significantly more $ST2^+$ cells compared to WT donor $T_R$, suggesting that the competitive advantage of YF and KO donor $T_R$ in chimeric VAT is in part due to an enhanced ability to access available IL-33 through increased ST2 expression. The transcriptional regulators BATF and IRF4 cooperate to induce expression of ST2 in $T_R$, possibly downstream of TCR signals as well as through IL-33 signaling itself (*12*). Additionally, IL-2 can work synergistically with IL-33 to upregulate ST2 and specifically expand $ST2^+$ $T_R$ (*60*, *61*). $T_R$ are unable to produce IL-2 themselves due to Foxp3-mediated transcriptional repression at the *Il2* locus (*62*, *63*) and therefore are dependent on paracrine sources of IL-2 produced by, for example, autoreactive $T_{eff}$ (*64*, *65*). However, KO $T_{eff}$ are defective in production of IL-2 compared to $T_{eff}$ from WT mice (*33*). The absence of an enriched population of ST2-expressing YF and KO VAT-$T_R$ at baseline may be explained by this lack of IL-2, which is rescued in the presence of WT IL-2 producing cells in mixed bone marrow chimeras.

Seemingly contradictory to our results, Molofsky *et al*. have argued that IL-33 signaling on $T_R$ in VAT is mediated through ICOS/ICOSL interactions with ILC2s and that absence of this interaction results in loss of VAT-$T_R$ (*66*). In their system, blockade of ICOS signaling was assessed in *Icosl*$^{-/-}$ mice, where cells are sufficient in ICOS expression though unable to interact with ligand. Consistent with their data in *Icosl*$^{-/-}$ mice, we did not observe any differences in ILC2 frequency or number in VAT of *Icos*$^{-/-}$ mice. However, given that ILC2s express both ICOS and ICOSL, loss of one versus the other could differentially impact ILC2 function, resulting in unique cell extrinsic impacts on $T_R$. Additionally, recent work investigating the molecular cues downstream of ICOS signaling revealed ligand-independent, constitutive signaling through PI3K-dependent pathways which relies on p85 association with the ICOS cytoplasmic YMFM motif and interactions between the ICOS transmembrane domain and the tyrosine kinase Lck (*28*, *67*). Thus the reported differences observed in our study and Molofsky's may be the result of low level, cell intrinsic PI3K activation in ICOS-expressing $T_R$ from *Icosl*$^{-/-}$ mice.

Although CCR2 plays an important role in recruitment of $T_R$ to VAT, we did not detect any differences in CCR2 expression in the absence of ICOS signaling. We did, however, observe a significantly increased frequency of $CCR3^+$ $T_R$ in the spleen and VAT of YF and KO mice, which was due to cell-intrinsic loss of ICOS signaling and was enhanced with age. CCR3 is primarily associated with type-2 responses (*68–72*), and lean, metabolically healthy VAT is maintained in an anti-inflammatory state by the presence of $T_H2$-associated cells. *In vivo* blockade of CCL11/24 resulted in a modest reduction of $T_R$ in YF VAT with no changes in other tissues analyzed. Parabiosis experiments demonstrate recruitment of circulating parabiont-derived $T_R$ to VAT after months of shared circulation (*39*, *40*), indicating that continual, low-level recruitment of

$T_R$ to VAT occurs throughout adulthood. Thus, longer-term antibody-mediated blockade may be necessary to observe significant effects on $T_R$ accumulation in our system. Additionally, addressing the role of CCR3 is further complicated by its promiscuity, and whether compensation through other ligands occurs during *in vivo* blockade is unknown. *In vitro*, we found that ICOS stimulation resulted in reduced CCR3 expression in WT VAT-$T_R$ with no changes in YF or KO cultures, suggesting that ICOS-dependent PI3K signaling can inhibit expression of CCR3. Regulation of CCR3 expression in T cells has not been extensively characterized, however there is evidence that the transcription factor GATA3 is able to bind to a regulatory region in the *Ccr3* locus (*73*). Nonlympohid $T_R$, including VAT-$T_R$, express high levels of GATA3 (*41*, *58*). However, whether ICOS signaling impacts CCR3 expression by modulating GATA3 expression or activity, and whether GATA3 is involved in controlling CCR3 expression in $T_R$, remains to be explored.

Most studies assessing VAT-$T_R$ biology utilize older male mice due to an increased abundance of canonical VAT-$T_R$ with age (*42*). However, various mediators of tissue inflammation, including IL-6, TNFα, and IL1β, are upregulated in the VAT of aged male mice (older than 24 weeks) (*74*). In our studies, we observed consistent accumulation of VAT-$T_R$ from 5 weeks on in all three genotypes, which was correlated with an increase in $CCR3^+$ $T_R$ up to ~20 weeks of age. CCR2 regulates T cell access to sites of inflammation (*47*), and studies assessing the contribution of CCR2 on $T_R$ migration to VAT utilize mice aged 25-30 weeks, when measures of VAT inflammation are increasing. CCR2 and CCR3 likely both have important roles for promoting recruitment of $T_R$ to VAT, however it will be necessary to evaluate whether these receptors are utilized differentially based on age, sex, and inflammation. For example, CCR3 may be important for early seeding and continuous recruitment of $T_R$ to VAT in comparatively younger mice when VAT inflammation is more minimal. With increasing age and inflammation (particularly in male mice), a switch to CCL2-CCR2 mediated migration may dominate.

Our work identifies new mechanisms that regulate VAT-$T_R$ biology. Here we describe a surprising, antagonistic role for ICOS-dependent PI3K signaling in the accumulation, prototypical phenotype, and function of $T_R$ specifically in VAT. We suggest that absence of ICOS signaling supports enhanced recruitment of $T_R$ to VAT via increased expression of CCR3. Further studies will be needed to identify the molecular mechanisms by which ICOS inhibits the VAT-$T_R$ phenotype and CCR3 expression. Our work highlights the complexity of tissue-specific $T_R$ development and accumulation and the importance of considering how signals from the immune environment elicit both cell- and tissue-specific effects.

## Materials and Methods

*Mice*

CD45.1$^{+}$ B6.SJL (B6.SJL-*Ptprc*$^{a}$*Pepc*$^{b}$/BoyJ), B6.*Icos*$^{-/-}$ (B6.129P2-*Icos*$^{tm1Mak}$/J), and B6.*Foxp3*$^{mRFP}$ (C57BL/6-*Foxp3*$^{tm1Flv}$/J) mice were purchased from The Jackson Laboratory. B6.*Icos*$^{Y181F}$ mice were provided by M. Pepper (University of Washington, Seattle, WA). CD45.1$^{+}$ B6.SJL mice were crossed to B6.*Foxp3*$^{mRFP}$ mice to generate *Foxp3*$^{mRFP}$ mice expressing CD45.1, CD45.2, and CD45.1/.2 allelic variants. B6.*Icos*$^{-/-}$ and B6.*Icos*$^{Y181F}$ mice were crossed to B6.*Foxp3*$^{mRFP}$ mice to generate B6.*Icos*$^{-/-}$ and B6.*Icos*$^{Y181F}$ mice expressing *Foxp3*$^{mRFP}$. All animals were bred and housed in specific pathogen-free conditions under the approval of the Institutional Animal Care and Use Committee of the Benaroya Research Institute. Males were used unless specified otherwise. Age of mice is indicated per experiment.

*Mixed bone marrow chimeras*

Bone marrow cells were prepared from donor mice by flushing femurs and tibias with PBS. Red blood cells (RBC) from filtered cells were lysed in ACK lysis buffer (Life Technologies) for 5 min at room temperature (RT). Recipient mice were lethally irradiated (2 x 600 rad separated by ≥4 hr). Mixed bone marrow chimeras were generated by retro-orbitally (r.o.) injecting a 1:1 ratio (≥2 x$10^{6}$ million cells total) of bone marrow cells of the appropriate genotypes into anesthetized recipient mice. Chimeric mice were rested for ≥10 wk.

*Intravascular labeling*

Mice were anesthetized with 4% isoflurane and 3 µg BV510- or BV650-conjugated CD45 (30-F11) was injected into mice r.o. in 200 µL PBS 5 min prior to sacrifice. Single cell suspensions were prepared for flow cytometry as described below, and localization of cells was determined by positive (blood-exposed) and negative (tissue-restricted) staining.

*Cell isolation*

Single-cell suspensions were prepared from spleen and peripheral LNs (pooled inguinal, axillary, brachial, and superficial cervical nodes) by tissue disruption with frosted glass slides into RPMI with 10% bovine calf serum (R-10, BCS) and filtered through nitex mesh. Blood was collected via cardiac puncture into PBS containing 2 mM EDTA. Epididymal visceral adipose (VAT) and inguinal subcutaneous adipose (SQAT) were excised, finely minced with scissors, and digested in RPMI basal medium with 0.14 U/mL Liberase TM (Roche) and 10 U/mL DNase I (Roche) for 30 min at 37°C with shaking (200 rpm). Supernatants were filtered through a 100 µM cell strainers and washed several times to remove mature adipocytes from the stromal vascular fraction. Ears were harvested for skin-infiltrating cells. Dorsal and ventral sides were separated using forceps and digested as described for VAT/SQAT for 45 min. Lungs were digested as described for skin. Large intestines were cleaned, stripped of fatty tissue, and inverted. Tissue was placed into extraction media (RPMI basal medium, 2 mM DTT, 1 mM EDTA, 2% BCS) and shaken at 37°C for 20 min to release intraepithelial lymphocytes (IEL). IEL-containing supernatant was removed and filtered into 50 mL conical tubes. For lamina propria lymphocyte (LPL) isolation, immediately following

incubation with extraction media, tissue was finely minced and placed into digestion media (RPMI basal media, 300 U/mL collagenase I [Worthington Biochemical Corporation], 1% BCS), shaken for 30 min at 37°C, and filtered into 50 mL conical tubes. Isolated cells from all tissues were incubated in ACK lysis buffer for 5 min, washed with R-10, and stained for flow cytometry or cultured for intracellular cytokine or chemokine receptor staining.

*Flow cytometry & intracellular cytokine staining*

Single-cell suspensions were stained with Fixable Viability Dye eFluor 780 (eBioscience) in PBS for 10 min at RT. For surface staining, cells were incubated at 4°C for 30 min in FACS buffer (PBS, 2% BCS) with directly conjugated antibodies (Abs) for murine proteins. Abs purchased from BioLegend unless noted: CD4 (RM4-5), CD8 (53-6.7), CD11b (M1/70), CD11c (N418), CD25 (PC61), CD44 (IM7), CD45 (30-F11), CD45.1 (A20), CD45.2 (104), CD62L (MEL-14), CD69 (H1.2F3), CD206 (C068C2), CXCR3 (CXCR3-173), F4/80 (BM8), Gr1 (RB6-8C5), ICOS (15F9), KLRG1 (2F1/KLRG1), Siglec-F (E50-2440; BD Biosciences), ST2 (U29-93; BD Biosciences), TCRβ (H57-597). For intracellular staining, cells were stained for surface antigens as described above, washed, and permeabilized for 20 min with eBioscience Fix/Perm buffer at 4°C. Cells were washed and stained in PermWash buffer (eBioscience) for 30 min at 4°C with Abs (purchased from BioLegend unless noted) against Bcl2 (BCL/10C4), CTLA-4 (UC10-4B9), Foxp3 (FJK-16s; Invitrogen), IFNγ (XMG1.2; BD Biosciences), IL-10 (JES5-16E3), Ki67 (11F6), TNFα (MP6-XT22). For intracellular cytokine staining following restimulation, cells were incubated in FACS tubes with PMA (50 ng/mL) and ionomycin (1 μg/mL) plus monensin (2 μM) in 0.3 mL complete RPMI medium (RPMI-C) [RPMI with 10% (vol/vol) fetal bovine serum, 100 U/mL penicillin, 100 μg/mL streptomycin, 25 μg/mL gentamycin, 1 mM sodium pyruvate, 10 mM HEPES, 2 mM L-glutamine, 55 μM β-ME] for 4 hr at 37°C, 5% $CO_2$ prior to staining as described above. Loss of mRFP expression occurred with our fixation/permeabilization protocols, requiring intracellular Foxp3 staining. Data were acquired on LSR II or FACSCanto flow cytometers (BD Biosciences) and analyzed using FlowJo software (TreeStar). Due to intraexperimental variability, geometric MFI was normalized as fold change compared to average expression in WT samples per experiment. Polybead polystyrene nonfluorescent microspheres (15 mm, Polysciences) were used to determine absolute cell numbers in flow cytometry samples. 100 μL of a fixed concentration ($C_B$) of beads was mixed with 100 μL cells to be counted. Samples were acquired on a flow cytometer, with gates drawn on lymphocyte and bead populations based on their forward- and side-scatter properties. The ratio of lymphocyte gate events ($N_L$) to bead gate events ($N_B$) was determined and used to calculate the concentration ($C_L$) of the original cell suspension as follows: $C_L = (N_L / N_B) \times C_B$

*Phospho-flow cytometry staining*

~1/4 of each spleen was immediately disrupted between frosted glass slides into BD Fix/Perm buffer (BD Biosciences). Cells were incubated for 20 min at RT, washed in FACS buffer, and resuspended in 90% ice cold methanol for ≥30 min. Cells were washed with BD Perm/Wash buffer (BD Biosciences) and stained for surface and

intracellular antigens, including p-S6 (D57.2.2E; Cell Signaling Technology) for 45 min at RT.

*Chemokine receptor staining*
Freshly isolated cells were incubated for 2.5 hr at 37°C, 5% $CO_2$ in RPMI-C. For CCR7 expression, cells were incubated with CCL19-human IgGFc fusion protein for 20 min at 4°C, washed, then incubated with PE-conjugated goat anti-human IgGFc (Jackson ImmunoResearch Laboratories) for 20 min at 4°C. To detect CCR2 (475301; R&D Systems) and CCR3 (J073E5; BioLegend), cells were incubated for 30 min at 37°C with directly conjugated antibodies diluted in FACS buffer. Cells were washed twice with FACS buffer before being acquired on the flow cytometer.

*Histology*
VAT was excised, immediately fixed in 10% formalin for 24 hr, then paraffin-embedded. Hematoxylin and eosin (H&E) staining was performed on 6 µm tissue sections by the Benaroya Research Institute Histology Core. Images were acquired using a Leica DM E compound microscope.

*RNA extraction and quantitative PCR*
VAT was dissected, immediately stabilized in RNAlater (Thermo Fisher), and frozen at -20°C until ready for processing. ~100 mg tissue was homogenized in 1 mL Qiazol and RNA was extracted using RNeasy Lipid Tissue Mini Kit (Qiagen) according to the manufacturer's instructions. RNA quality and quantity was determined using an ND-1000 spectrophotometer (NanoDrop, Thermo Fisher). 500 ng template RNA was reverse transcribed with random hexamer primers in 20 µL using RevertAid First Strand cDNA Synthesis Kit (Thermo Fisher) and subsequently diluted 1:3.3 with nuclease-free water. qPCR was performed using 2 µL diluted cDNA and presynthesized TaqMan Gene Expression assays in TaqMan Gene Expression Master Mix (Applied Biosystems) for amplification of the following transcripts in a final volume of 20 µL: *Ccl5* (Mm01302427_m1), *Ccl7* (Mm00443113_m1), *Ccl11* (Mm0441238_m1), *Ccl24* (Mm00444701_m1), and *Ccl26* (Mm02763057_u1). Samples were run in technical triplicates using the QuantStudio 5 Real-Time PCR System (Thermo Fisher) with 10 min initial activation at 95°C followed by 40 cycles of 15 sec at 95°C, 60 sec at 60°C. Mean target mRNA levels were calculated by ΔΔCT method and normalized to Tbp (Mm01277042_m1) expression using QuantStudio Design and Analysis Software (Thermo Fisher).

*In vitro stimulation of VAT T cells*
VAT was pooled from 2-3 mice of the same genotype to ensure adequate cell number for culture. Cells were isolated as described above, and $CD4^+$ T cells were enriched by incubating cells with CD4 MicroBeads and positively selecting with MACS cell separation MS columns (Miltenyi Biotec). Purified cells were resuspended in RPMI-C with 500 U/mL recombinant IL-2 (eBioscience). Cells were cultured for 48 hr in 96-well flat-bottom plates with plate-bound αCD3 (2C11) and αCD28 (37.51) from Bio X Cell at 1 µg/µL, with or without the addition of plate-bound αICOS (C398.4A; BioLegend) at 2 µg/µL. Expression of CCR3 was assessed by flow cytometry as described above.

*In vivo antibody blockade*
Mice aged 8-10 weeks were given 0.75 µg/g body weight αCCL11 and αCCL24 (R&D Systems; MAB420 and MAB528) or an equivalent amount of rat IgG (Sigma) diluted in PBS by intraperitoneal (i.p.) injection on days 0, 5, and 10 and sacrificed for analysis on day 13.

*High-fat diet*
Mice were placed on 18-week HFD (60% kcal fat diet, Research Diets D124928, *ad libitum*) beginning at 5-7 weeks of age. Weights and blood glucose (BGL) by tail prick (Contour Next One glucose meter; Ascensia Diabetes Care) were taken weekly after 6 hr of fasting.

*Insulin and glucose tolerance tests*
Insulin tolerance tests were performed in conscious mice fasted for 6 hr. 1 U/kg human insulin (Sigma) was given i.p. and blood was collected by tail prick for BGL at 0, 15, 30, 45, and 60 min post insulin administration. Three days later, glucose tolerance tests were performed in conscious mice fasted for 6 hr. 1 g/kg glucose (Sigma) was administered i.p. Blood was collected by tail prick for BGL at 0, 15, 30, 60, 90, and 120 min post-glucose bolus .

*Statistical analysis*
All data are presented as mean values ± SD and graphs were created and analyzed using Prism Software (GraphPad). Comparisons between genotypes were analyzed using one- or two-way ANOVA where appropriate, adjusted for multiple comparisons using Tukey's post-test. For mixed bone marrow chimeras, statistical significance was determined using two-tailed paired Student's *t* tests when comparing cells within the same chimeric mouse.

**Acknowledgements**

We thank A. Wojno, K. Arumuganathan, and T. Nguyen for maintaining the BRI Flow Cytometry Core; P. Johnson in the BRI Histology/Imaging Core; and D. Hackney and S. Zraika from the UW Diabetes Research Center Cell Function Analysis Core for help with metabolic profiling tests. M. Pepper generously provided *Icos*$^{Y181F}$ mice with kind permission from Woong-Kyung Suh. A. Burich, C. Toledano, and the BRI vivarium staff helped maintain mouse colonies. We thank members of the Campbell lab for helpful discussion and laboratory support.

This work was supported by grants to D.J.C. from the National Institutes of Health (NIH) (R01AI124693, R01AI136475). K.L.M. was supported by NIH National Institute of Allergy and Infectious Diseases T32 Grant AI106677, National Institute of General Medical Sciences T32 Grant GM007270, and the UW Diabetes Research Center Samuel and Althea Stroum Endowed Graduate Fellowship (2P30 DK17047).

Author Contributions: K.L.M. and D.J.C. conceptualized study and designed experiments. K.L.M. performed experiments, analyzed data, and wrote original draft. D.J.C. reviewed and edited.

Disclosures: The authors declare no competing financial interests.

**References**

1. M. Dominguez-Villar, D. A. Hafler, Regulatory T cells in autoimmune disease. *Nat. Immunol.* **19**, 665–675 (2018).

2. M. N. Rivas, T. A. Chatila, Regulatory T cells in allergic diseases. *J. Allergy Clin. Immunol.* **138**, 639–652 (2016).

3. K. S. Smigiel, S. Srivastava, J. M. Stolley, D. J. Campbell, Regulatory T-cell homeostasis: steady-state maintenance and modulation during inflammation. *Immunol. Rev.* **259**, 40–59 (2014).

4. D. Burzyn, W. Kuswanto, D. Kolodin, J. L. Shadrach, M. Cerletti, Y. Jang, E. Sefik, T. G. Tan, A. J. Wagers, C. Benoist, and D. Mathis, A special population of regulatory T cells potentiates muscle repair. *Cell* **155**, 1282–1295 (2013).

5. N. Arpaia, J. A. Green, B. Moltedo, A. Arvey, S. Hemmers, S. Yuan, P. M. Treuting, A. Y. Rudensky, A distinct function of regulatory T cells in tissue protection. *Cell* **162**, 1078–1089 (2015).

6. N. Ali, B. Zirak, R. Rodriguez, M. Pauli, H.-A. Truong, K. Lai, R. Ahn, K. Corbin, M. Lowe, T. Scharschmidt, K. Taravati, M. Tan, R. Ricardo-Gonzalez, A. Nosbaum, M. Bertolini, W. Liao, F. Nestle, R. Paus, G. Cotsarelis, A. Abbas, M. Rosenblum, Regulatory T cells in skin facilitate epithelial stem cell differentiation. *Cell* **169**, 1119–1129 (2017).

7. L. A. Kalekar, J. N. Cohen, N. Prevel, P. M. Sandoval, A. N. Mathur, J. M. Moreau, M. M. Lowe, A. Nosbaum, P. J. Wolters, A. Haemel, F. Boin, and M. D. Rosenblum, Regulatory T cells in skin are uniquely poised to suppress profibrotic immune responses. *Sci. Immunol*. **4**, eaaw2910 (2019).

8. M. Feuerer, L. Herrero, D. Cipolletta, A. Naaz, J. Wong, A. Nayer, J. Lee, A. Goldfine, C. Benoist, S. Shoelson. D. Mathis, Lean, but not obese, fat is enriched for a unique population of regulatory T cells that affect metabolic parameters. *Nat. Med.* **15**, 930–939 (2009).

9. J. Deiuliis, Z. Shah, N. Shah, B. Needleman, D. Mikami, V. Narula, K. Perry, J. Hazey, T. Kampfrath, M. Kollengode, Q. Sun, A. R. Satoskar, C. Lumeng, S. Moffatt-Bruce, S. Rajagopalan, Visceral adipose inflammation in obesity is associated with critical alterations in Tregulatory cell numbers. *PLoS One* **6**, e16376 (2011).

10. Y. Ilan, R. Maron, A.-M. Tukpah, T. Maioli, G. Murugaiyan, K. Yang, H. Wu, H. Weiner, Induction of regulatory T cells decreases adipose inflammation and alleviates insulin resistance in ob/ob mice. *Proc. Nat. Acad. Sci.* **107**, 9765–9770 (2010).

11. K. Eller, A. Kirsch, A. M. Wolf, S. Sopper, A. Tagwerker, U. Stanzl, D. Wolf, W. Patsch, A. R. Rosenkranz, P. Eller, Potential role of regulatory T cells in reversing obesity-linked insulin resistance and diabetic nephropathy. *Diabetes* **60**, 2954–2962 (2011).

12. A. Vasanthakumar, K. Moro, A. Xin, Y. Liao, R. Gloury, S. Kawamoto, S. Fagarasan, L. Mielke, S. Afshar-Sterle, S. Masters, S. Nakae, H. Saito, J. Wentworth, P. Li, W. Liao, W. Leonard, G. Smyth, W. Shi, S. Nutt, S. Koyasu, A. Kallies, The transcriptional regulators IRF4, BATF and IL-33 orchestrate development and maintenance of adipose tissue-resident regulatory T cells. *Nat. Immunol.* **16**, 276–285 (2015).

13. J. M. Han, D. Wu, H. C. Denroche, Y. Yao, C. B. Verchere, M. K. Levings, IL-33 reverses an obesity-induced deficit in visceral adipose tissue ST2+ T regulatory cells and ameliorates adipose tissue inflammation and insulin resistance. *J. Immunol.* **194**, 4777–4783 (2015).

14. K. S. Smigiel, E. Richards, S. Srivastava, K. R. Thomas, J. C. Dudda, K. D. Klonowski, D. J. Campbell, CCR7 provides localized access to IL-2 and defines homeostatically distinct regulatory T cell subsets. *J. Exp. Med*. **211**, 121–136 (2014).

15. D. J. Campbell, Control of regulatory T cell migration, function, and homeostasis. *J. Immunol.* **195**, 2507–2513 (2015).

16. C. T. Luo, W. Liao, S. Dadi, A. Toure, M. O. Li, Graded Foxo1 activity in Treg cells differentiates tumour immunity from spontaneous autoimmunity. *Nature* **529**, 532–536 (2016).

17. M. Delacher, C. Imbusch, D. Weichenhan, A. Breiling, A. Hotz-Wagenblatt, U. Träger, A.-C. Hofer, D. Kägebein, Q. Wang, F. Frauhammer, J.-P. Mallm, K. Bauer, C. Herrmann, P. Lang, B. Brors, C. Plass, M. Feuerer, Genome-wide DNA-methylation landscape defines specialization of regulatory T cells in tissues. *Nat. Immunol.* **18**, 1160–1172 (2017).

18. J. R. DiSpirito, D. Zemmour, D. Ramanan, J. Cho, R. Zilionis, A. M. Klein, C. Benoist, D. Mathis, Molecular diversification of regulatory T cells in non-lymphoid tissues. *Sci. Immunol.* **3**, eaat5861 (2018).

19. B. D. Sather, P. Treuting, N. Perdue, M. Miazgowicz, J. D. Fontenot, A. Y. Rudensky, D. J. Campbell, Altering the distribution of Foxp3(+) regulatory T cells results in tissue-specific inflammatory disease. *J. Exp. Med.* **204**, 1335–1347 (2007).

20. T. Yamaguchi, J. B. Wing, S. Sakaguchi, Two modes of immune suppression by Foxp3$^{+}$ regulatory T cells under inflammatory or non-inflammatory conditions. *Sem. Immunol.* **23**, 424–430 (2011).

21. A. G. Levine, A. Arvey, W. Jin, A. Y. Rudensky, Continuous requirement for the TCR in regulatory T cell function. *Nat. Immunol.* **15**, 1070–1078 (2014).

22. Q. Tang, K. J. Henriksen, E. K. Boden, A. J. Tooley, J. Ye, S. K. Subudhi, X. X. Zheng, T. B. Strom, J. A. Bluestone, Cutting edge: CD28 controls peripheral homeostasis of CD4+CD25+ regulatory T cells. *J. Immunol.* **171**, 3348–3352 (2003).

23. S. Redpath, N. van der Werf, A. Cervera, A. MacDonald, D. Gray, R. Maizels, M. Taylor, ICOS controls Foxp3(+) regulatory T-cell expansion, maintenance and IL-10 production during helminth infection. *Eur. J. Immunol*. **43**, 705–715 (2013).

24. Y. Burmeister, T. Lischke, A. C. Dahler, H. W. Mages, K.-P. P. Lam, A. J. Coyle, R. A. Kroczek, A. Hutloff, ICOS controls the pool size of effector-memory and regulatory T cells. *J. Immunol.* **180**, 774–782 (2008).

25. E. Cretney, A. Xin, W. Shi, M. Minnich, F. Masson, M. Miasari, G. T. Belz, G. K. Smyth, M. Busslinger, S. L. Nutt, A. Kallies, The transcription factors Blimp-1 and IRF4 jointly control the differentiation and function of effector regulatory T cells. *Nat. Immunol.* **12**, 304–311 (2011).

26. Y. Arimura, H. Kato, U. Dianzani, T. Okamoto, S. Kamekura, D. Buonfiglio, T. Miyoshi-Akiyama, T. Uchiyama, J. Yagi, A co-stimulatory molecule on activated T cells, H4/ICOS, delivers specific signals in T(h) cells and regulates their responses. *Int. Immunol.* **14**, 555–566 (2002).

27. A. Hutloff, A. Dittrich, K. Beier, B. Eljaschewitsch, R. Kraft, I. Anagnostopoulos, R. Kroczek. ICOS is an inducible T-cell co-stimulator structurally and functionally related to CD28. *Nature* **397**, 263–266 (1999).

28. M. Feito, R. Vaschetto, G. Criado, A. Sánchez, A. Chiocchetti, A. Jiménez-Periáñez, U. Dianzani, P. Portoles, J. Rojo, Mechanisms of H4/ICOS costimulation: effects on proximal TCR signals and MAP kinase pathways. *Eur. J. Immunol*. **33**, 204–214 (2003).

29. N. Okamoto, K. Tezuka, M. Kato, R. Abe, T. Tsuji, PI3-kinase and MAP-kinase signaling cascades in AILIM/ICOS- and CD28-costimulated T-cells have distinct functions between cell proliferation and IL-10 production. *Biochem. Biophys. Res. Commun.* **310**, 691–702 (2003).

30. A. Herman, G. Freeman, D. Mathis, C. Benoist, CD4+CD25+ T regulatory cells dependent on ICOS promote regulation of effector cells in the prediabetic Lesion. *J. Exp. Med.* **199**, 1479–1489 (2004).

31. M. Kornete, E. Sgouroudis, C. A. Piccirillo, ICOS-dependent homeostasis and function of Foxp3+ regulatory T cells in islets of nonobese diabetic mice. *J. Immunol.* **188**, 1064–1074 (2012).

32. M. Busse, M. Krech, A. Meyer-Bahlburg, C. Hennig, G. Hansen, ICOS mediates the generation and function of CD4+CD25+Foxp3+ regulatory T cells conveying respiratory tolerance. *J. Immunol.* **189**, 1975–1982 (2012).

33. C. Dong, A. E. Juedes, U. A. Temann, S. Shresta, J. P. Allison, N. H. Ruddle, R. A. Flavell, ICOS co-stimulatory receptor is essential for T-cell activation and function. *Nature* **409**, 97–101 (2001).

34. A. Landuyt, B. Klocke, T. Colvin, T. Schoeb, C. Maynard, Cutting Edge: ICOS-deficient regulatory T cells display normal induction of Il10 but readily downregulate expression of Foxp3. *J. Immunol.* **202**, 1039–1044 (2019).

35. M. Kohyama, D. Sugahara, S. Sugiyama, H. Yagita, K. Okumura, N. Hozumi, Inducible costimulator-dependent IL-10 production by regulatory T cells specific for self-antigen. *Proc. Natl. Acad. Sci. U.S.A.* **101**, 4192–4197 (2004).

36. K. Miyamoto, C. Kingsley, X. Zhang, C. Jabs, L. Izikson, R. Sobel, H. Weiner, V. Kuchroo, A. Sharpe, ICOS molecule plays a crucial role in the development of mucosal tolerance. *J. Immunol.* **175**, 7341–7347 (2005).

37. C. Fos, A. Salles, V. Lang, F. Carrette, S. Audebert, S. Pastor, M. Ghiotto, D. Olive, G. Bismuth, J. A. Nunès, ICOS ligation recruits the p50alpha PI3K regulatory subunit to the immunological synapse. *J. Immunol.* **181**, 1969–1977 (2008).

38. L. So, and D. A. Fruman, PI3K signalling in B- and T-lymphocytes: new developments and therapeutic advances. *Biochem. J.* **442**, 465–481 (2012).

39. D. Kolodin, N. van Panhuys, C. Li, A. M. Magnuson, D. Cipolletta, C. M. Miller, A. Wagers, R. N. Germain, C. Benoist, D. Mathis, Antigen- and cytokine-driven accumulation of regulatory T cells in visceral adipose tissue of lean mice. *Cell. Metab.* **21**, 543–557 (2015).

40. A. Vasanthakumar., D. Chisanga, J. Blume, R. Gloury, K. Britt, D. C. Henstridge, Y. Zhan, S. V. Torres, S. Liene, N. Collins, E. Cao, T. Sidwell, C. Li, R. G. Spallanzani, Y. Liao, P. A. Beavis, T. Gebhardt, N. Trevaskis, S. L. Nutt, J. D. Zajac, R. A. Davey, M. A. Febbraio, D. Mathis, W. Shi, A. Kallies, Sex-specific adipose tissue imprinting of regulatory T cells. *Nature* **579**, 581–585 (2020).

41. D. Cipolletta, M. Feuerer, A. Li, N. Kamei, J. Lee, S. E. Shoelson, C. Benoist, D. Mathis, PPAR-γ is a major driver of the accumulation and phenotype of adipose tissue Treg cells. *Nature* **486**, 549–553 (2012).

42. D. Cipolletta, P. Cohen, B. M. Spiegelman, C. Benoist, D. Mathis, Appearance and disappearance of the mRNA signature characteristic of Treg cells in visceral adipose tissue: age, diet, and PPARγ effects. *Proc. Natl. Acad. Sci. U.S.A.* **112**, 482–487 (2015).

43. M. Gigoux, J. Shang, Y. Pak, M. Xu, J. Choe, T. W. Mak, W.-K. K. Suh, Inducible costimulator promotes helper T-cell differentiation through phosphoinositide 3-kinase. *Proc. Natl. Acad. Sci. U.S.A.* **106**, 20371–20376 (2009).

44. Y. Y. Wan, R. A. Flavell, Identifying Foxp3-expressing suppressor T cells with a bicistronic reporter. *Proc. Natl. Acad. Sci. U.S.A.* **102**, 5126–5131 (2005).

45. T. Nishioka, J. Shimizu, R. Iida, S. Yamazaki, S. Sakaguchi, CD4+ CD25+ Foxp3+ T cells and CD4+ CD25− Foxp3+ T cells in aged mice. *J. Immunol.* **176**: 6586–6593 (2006).

46. Y. M. Kerdiles, D. R. Beisner, R. Tinoco, A. S. Dejean, D. H. Castrillon, R. A. DePinho, S. M. Hedrick, Foxo1 links homing and survival of naive T cells by regulating L-selectin, CCR7 and interleukin 7 receptor. *Nat. Immunol.* **10**, 176–184 (2009).

47. J. H. Lee, S. G. Kang, C. H. Kim, FoxP3+ T cells undergo conventional first switch to lymphoid tissue homing receptors in thymus but accelerated second switch to nonlymphoid tissue homing receptors in secondary lymphoid tissues. *J. Immunol.* **178**, 301–311 (2007).

48. K. Anderson, K. Mayer-Barber, H. Sung, L. Beura, B. James, J. Taylor, L. Qunaj, T. Griffith, V. Vezys, D. Barber, D. Masopust, Intravascular staining for discrimination of vascular and tissue leukocytes. *Nat. Protoc.* **9**, 209–222 (2014).

49. H. Ahnstedt, M. Roy-O'Reilly, M. S. Spychala, A. S. Mobley, J. Bravo-Alegria, A. Chauhan, J. Aronowski, S. P. Marrelli, L. D. McCullough, Sex differences in adipose tissue CD8+ T cells and regulatory T cells in middle-aged mice. *Front. Immunol.* **9**, 659 (2018).

50. U. Pettersson, T. Waldén, P.-O. Carlsson, L. Jansson, M. Phillipson, Female mice are protected against high-fat diet induced metabolic syndrome and increase the regulatory T cell population in adipose tissue. *PLoS One* **7**, e46057 (2012).

51. C. Li, J. R. DiSpirito, D. Zemmour, R. G. Spallanzani, W. Kuswanto, C. Benoist, D. Mathis, TCR transgenic mice reveal stepwise, multi-site acquisition of the distinctive fat-Treg phenotype. *Cell* **174**, 285–299 (2018).

52. A. Molofsky, J. Nussbaum, H.-E. Liang, S. Dyken, L. Cheng, A. Mohapatra, A. Chawla, R. Locksley, Innate lymphoid type 2 cells sustain visceral adipose tissue eosinophils and alternatively activated macrophages. *J. Exp. Med.* **210**, 535–549 (2013).

53. M. S. Burhans, D. K. Hagman, J. N. Kuzma, K. A. Schmidt, M. Kratz, Contribution of adipose tissue inflammation to the development of type 2 diabetes mellitus. *Compr. Physiol.* **9**, 1–58 (2018).

54. J. Schmitz, A. Owyang, E. Oldham, Y. Song, E. Murphy, T. K. McClanahan, G. Zurawski, M. Moshrefi, J. Qin, X. Li, D. M. Gorman, J. F. Bazan, R. A. Kastelein, IL-33, an interleukin-1-like cytokine that signals via the IL-1 receptor-related protein ST2 and induces T helper type 2-associated cytokines. *Immunity* **23**, 479–490 (2005).

55. D. Wu, A. B. Molofsky, H.-E. E. Liang, R. R. Ricardo-Gonzalez, H. A. Jouihan, J. K. Bando, A. Chawla, R. M. Locksley, Eosinophils sustain adipose alternatively activated macrophages associated with glucose homeostasis. *Science* **332**, 243–247 (2011).

56. V. Panneton, J. Chang, M. Witalis, J. Li, W.-K. Suh, Inducible T-cell co-stimulator : signaling mechanisms in T follicular helper cells and beyond. *Immunol. Rev.* **291**, 91–103 (2019).

57. N. Komatsu, S. Hori, Full restoration of peripheral Foxp3+ regulatory T cell pool by radioresistant host cells in scurfy bone marrow chimeras. *Proc. Natl. Acad. Sci. U.S.A.* **104**, 8959–8964 (2007).

58. M. Delacher, C. Imbusch, A. Hotz-Wagenblatt, J.-P. Mallm, K. Bauer, M. Simon, D. Riegel, A. Rendeiro, S. Bittner, L. Sanderink, A. Pant, L. Schmidleithner, K. Braband, B. Echtenachter, A. Fischer, V. Giunchiglia, P. Hoffmann, M. Edinger, C. Bock, M. Rehli, B. Brors, C. Schmidl, M. Feuerer, Precursors for nonlymphoid-tissue Treg cells reside in secondary lymphoid organs and are programmed by the transcription factor BATF. *Immunity* **52**,1–18 (2020).

59. C. A. O'Brien, S. J. Batista, K. M. Still, T. H. Harris, IL-10 and ICOS differentially regulate T cell responses in the brain during chronic *Toxoplasma gondii* infection. *J. Immunol*. **202**, 1755–1766 (2019).

60. L. Guo, G. Wei, J. Zhu, W. Liao, W. J. Leonard, K. Zhao, W. Paul, IL-1 family members and STAT activators induce cytokine production by Th2, Th17, and Th1 cells. *Proc. Natl. Acad. Sci. U.S.A.* **106**, 13463–13468 (2009).

61. B. M. Matta, J. M. Lott, L. R. Mathews, Q. Liu, B. R. Rosborough, B. R. Blazar, H. R. R. Turnquist, IL-33 is an unconventional alarmin that stimulates IL-2 secretion by dendritic cells to selectively expand IL-33R/ST2+ regulatory T cells. *J. Immunol.* **193**, 4010–4020 (2014).

62. Y. Wu, M. Borde, V. Heissmeyer, M. Feuerer, A. Lapan, J. Stroud, D. Bates, L. Guo, A. Han, S. Ziegler, D. Mathis, C. Benoist, L. Chen, A. Rao, FOXP3 controls regulatory T cell function through cooperation with NFAT. *Cell* **126**, 375–387 (2006).

63. M. Ono, H. Yaguchi, N. Ohkura, I. Kitabayashi, Y. Nagamura, T. Nomura, Y. Miyachi, T. Tsukada, S. Sakaguchi, Foxp3 controls regulatory T-cell function by interacting with AML1/Runx1. *Nature* **446**, 685–689 (2007).

64. R. Setoguchi, S. Hori, T. Takahashi, S. Sakaguchi, Homeostatic maintenance of natural Foxp3(+) CD25(+) CD4(+) regulatory T cells by interleukin (IL)-2 and induction of autoimmune disease by IL-2 neutralization. *J. Exp. Med.* **201**, 723–735 (2005).

65. J. M. Stolley, D. J. Campbell, A 33D1+ dendritic cell/autoreactive CD4+ T cell circuit maintains IL-2-dependent regulatory T cells in the spleen. *J. Immunol.* **197**, 2635–2645 (2016).

66. A. B. Molofsky, F. Van Gool, H.-E. E. Liang, S. J. Van Dyken, J. C. Nussbaum, J. Lee, J. A. Bluestone, R. M. Locksley, Interleukin-33 and Interferon-γ counter-regulate group 2 innate lymphoid cell activation during immune perturbation. *Immunity* **43**, 161–174 (2015).

67. Z. Wan, X. Shao, X. Ji, L. Dong, J. Wei, Z. Xiong, W. Liu, H. Qi, Transmembrane domain-mediated Lck association underlies bystander and costimulatory ICOS signaling. *Cell & Mol. Immunol.* **17**, 143–152 (2020).

68. E. Danilova, I. Skrindo, E. Gran, B. J. Hales, W. A. Smith, J. Jahnsen, F. E. Johansen, F. L. Jahnsen, E. S. Baekkevold, A role for CCL28–CCR3 in T-cell homing to the human upper airway mucosa. *Nat. Mucosal Immunol*. **8**, 107–114 (2015).

69. J. N. Francis, C. M. Lloyd, I. Sabroe, S. R. Durham, S. J. Till, T lymphocytes expressing CCR3 are increased in allergic rhinitis compared with non-allergic controls and following allergen immunotherapy. *Allergy* **62**, 59–65 (2007).

70. D. Nagakubo, O. Yoshie, T. Hirata, Upregulated CCL28 expression in the nasal mucosa in experimental allergic rhinitis: Implication for CD4+ memory T cell recruitment. *Cell. Immunol.* **302**, 58–62 (2016).

71. W. Ma, P. J. Bryce, A. A. Humbles, D. Laouini, A. Yalcindag, H. Alenius, D. S. Friend, H. C. Oettgen, C. Gerard, R. S. Geha, CCR3 is essential for skin eosinophilia and airway hyperresponsiveness in a murine model of allergic skin inflammation. *J. Clin. Invest.* **109**, 621–628 (2002).

72. A. A. Humbles, B. Lu, D. S. Friend, S. Okinaga, J. Lora, A. Algarawi, T. R. Martin, N. P. Gerard, C. Gerard, The murine CCR3 receptor regulates both the role of eosinophils and mast cells in allergen-induced airway inflammation and hyperresponsiveness. *Proc. Natl. Acad. Sci. U.S.A.* **99**, 1479–1484 (2002).

73. S.-K. K. Kong, B. S. Kim, T. G. Uhm, W. Lee, G. R. Lee, C.-S. S. Park, C.-H. H. Lee, I. Y. Chung, Different GATA factors dictate CCR3 transcription in allergic inflammatory cells in a cell type-specific manner. *J. Immunol.* **190**, 5747–5756 (2013).

74. D. Wu, Z. Ren, M. Pae, W. Guo, X. Cui, A. H. Merrill, S. N. Meydani, Aging up-regulates expression of inflammatory mediators in mouse adipose tissue. *J. Immunol.* **179**, 4829–4839 (2007).

## Abbreviations

| | |
|---|---|
| ATM | Adipose tissue macrophage |
| BGL | Blood glucose level |
| $cT_R$ | Central regulatory T cell |
| $eT_R$ | Effector regulatory T cell |
| HFD | High-fat diet |
| ILC2 | Type 2 innate lymphoid cell |
| KO | *Icos*$^{-/-}$ |
| PI3K | Phosphoinositide 3-kinase |
| SQAT | Subcutaneous adipose tissue |
| $T_{eff}$ | Effector T cell |
| $T_R$ | Regulatory T cell |
| VAT | Visceral adipose tissue |
| YF | *Icos*$^{Y181F}$ |

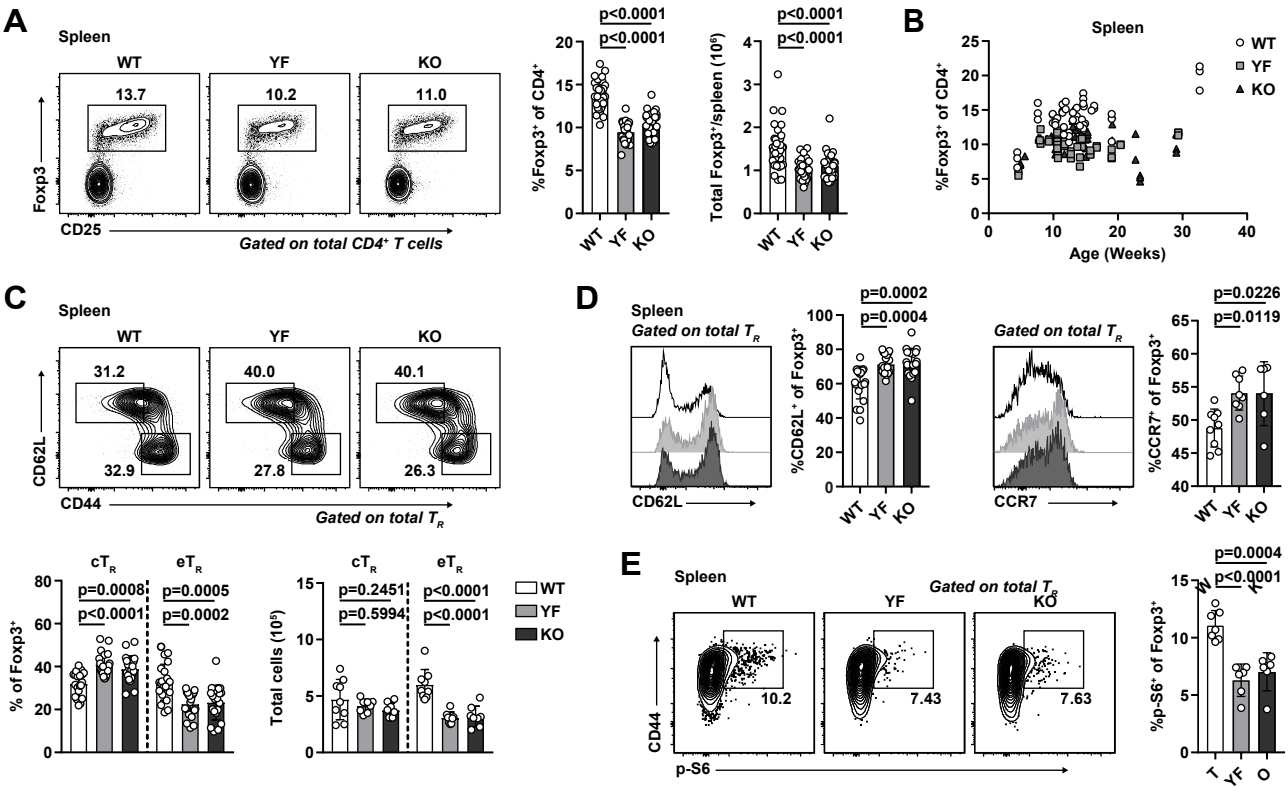


**Figure 1: Absence of ICOS signaling results in loss of lymphoid $T_R$ and altered expression of PI3K targets. (A)** Splenic $T_R$ frequencies of total $CD4^+$ T cells in WT, YF, and KO mice as measured by flow cytometry. Graphical data shows splenic $T_R$ frequencies (left graph) and total $T_R$ number (right graph). **(B)** Splenic $T_R$ frequencies at indicated mouse ages. Each point represents data from one mouse. **(C)** Abundance of $cT_R$ ($CD44^{lo}CD62L^{hi}$) and $eT_R$ ($CD44^{hi}CD62L^{lo}$) populations of total splenic $T_R$ as measured by flow cytometry with graphical data of $cT_R$ and $eT_R$ frequencies (bottom left graph) and total splenic $cT_R$ and $eT_R$ (bottom right graph). **(D)** Expression of CD62L and CCR7 in gated splenic $T_R$. **(E)** S6 phosphorylation measured directly *ex vivo* in splenic $T_R$ by flow cytometry. Flow cytometry plots are representative of data from 2 or more independent experiments. Graphical data are compiled from 2 or more independent experiments using mice aged 8-16 weeks, with $n$ = 3-5 mice per group per experiment. Statistical significance was determined using one-way ANOVA with Tukey's post-test. All graphical data are presented as mean values ± SD.

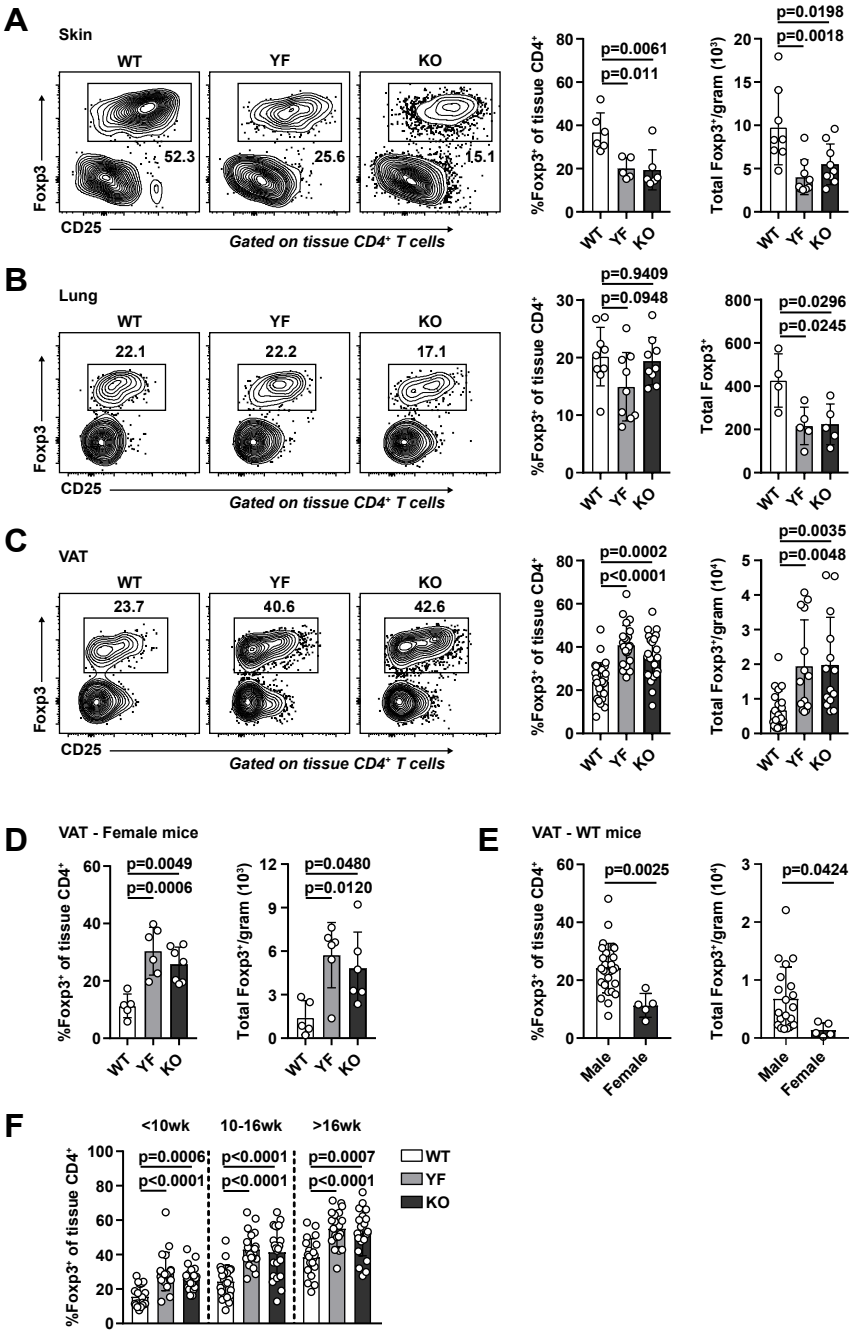


**Figure 2: $T_R$ frequency and number are increased in VAT in the absence of ICOS signaling. (A-C)** Representative flow cytometry plots showing frequency of $T_R$ among tissue-localized TCRβ⁺CD4⁺ cells in WT, YF, and KO ear skin **(A)**, lung **(B)**, and VAT **(C)**. Pooled data from mice 8-16 weeks old with $T_R$ frequencies (left graphs) and total $T_R$ number (right graphs) of aforementioned tissues. **(D)** $T_R$ frequency of tissue-localized CD4⁺ T cells (left) and total $T_R$ number (right) in VAT of female WT, YF, and KO mice. **(E)** $T_R$ frequency (left) and total $T_R$ number (right) in VAT of 8-16 week old male and female WT mice. **(F)** VAT-$T_R$ frequencies by noted age bins as measured by flow cytometry. Flow cytometry plots are representative of data from 2 or more independent experiments. Graphical data are compiled from 2 or more independent experiments with *n* = 2-5 mice per group per experiment. Statistical significance was determined using one-way ANOVA with Tukey's post-test or two-tailed Student's *t* test where appropriate. All data are presented as mean values ± SD.

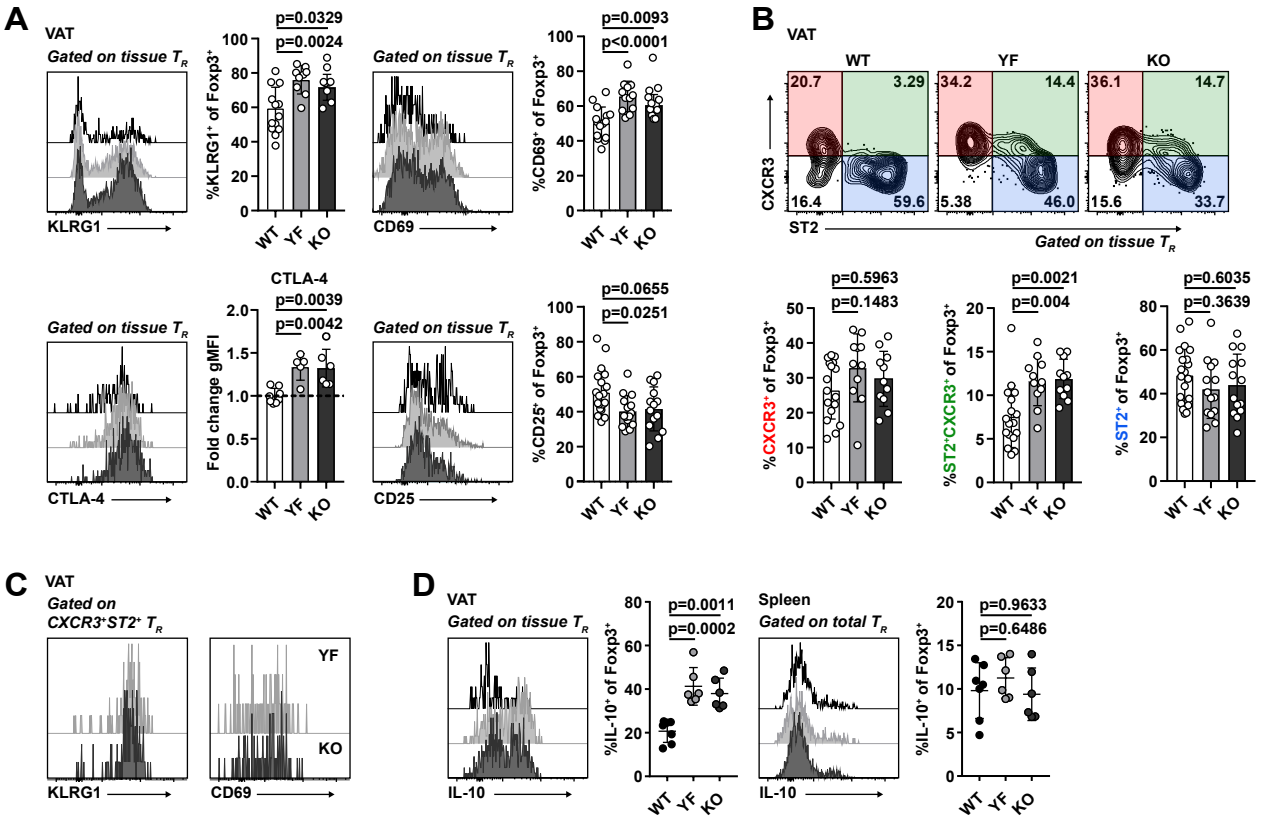


**Figure 3: Loss of ICOS signaling supports an e$T_R$ phenotype in VAT. (A)** Representative flow cytometry plots and summarized graphical data of KLRG1, CD69, CTLA-4, and CD25 expression in tissue-localized VAT-$T_R$. CTLA-4 geometric MFI was calculated as fold change compared to average expression in WT $T_R$ for each individual experiment. **(B)** Representative gating of VAT-$T_R$ on CXCR3 and ST2 expression. Graphs summarize the frequency of WT, YF, and KO VAT-$T_R$ positive for CXCR3 (left) or ST2 (right) alone, or double-expressers of CXCR3 and ST2 (middle). **(C)** Histograms showing expression of KLRG1 and CD69 in CXCR3$^+$ST2$^+$ YF and KO VAT-$T_R$ as measured by flow cytometry. **(D)** Representative flow cytometry plots and summarized graphical data showing IL-10 expression in $T_R$ from VAT and spleen after 4h PMA/I+monensin stimulation *ex vivo*. Flow cytometry plots are representative of data from 2 or more independent experiments. Graphical data are compiled from 2 or more independent experiments using 8-16 week old mice, with *n* = 3-5 mice per group per experiment. Statistical significance was determined using one-way ANOVA with Tukey's post-test. All data are presented as mean values ± SD.

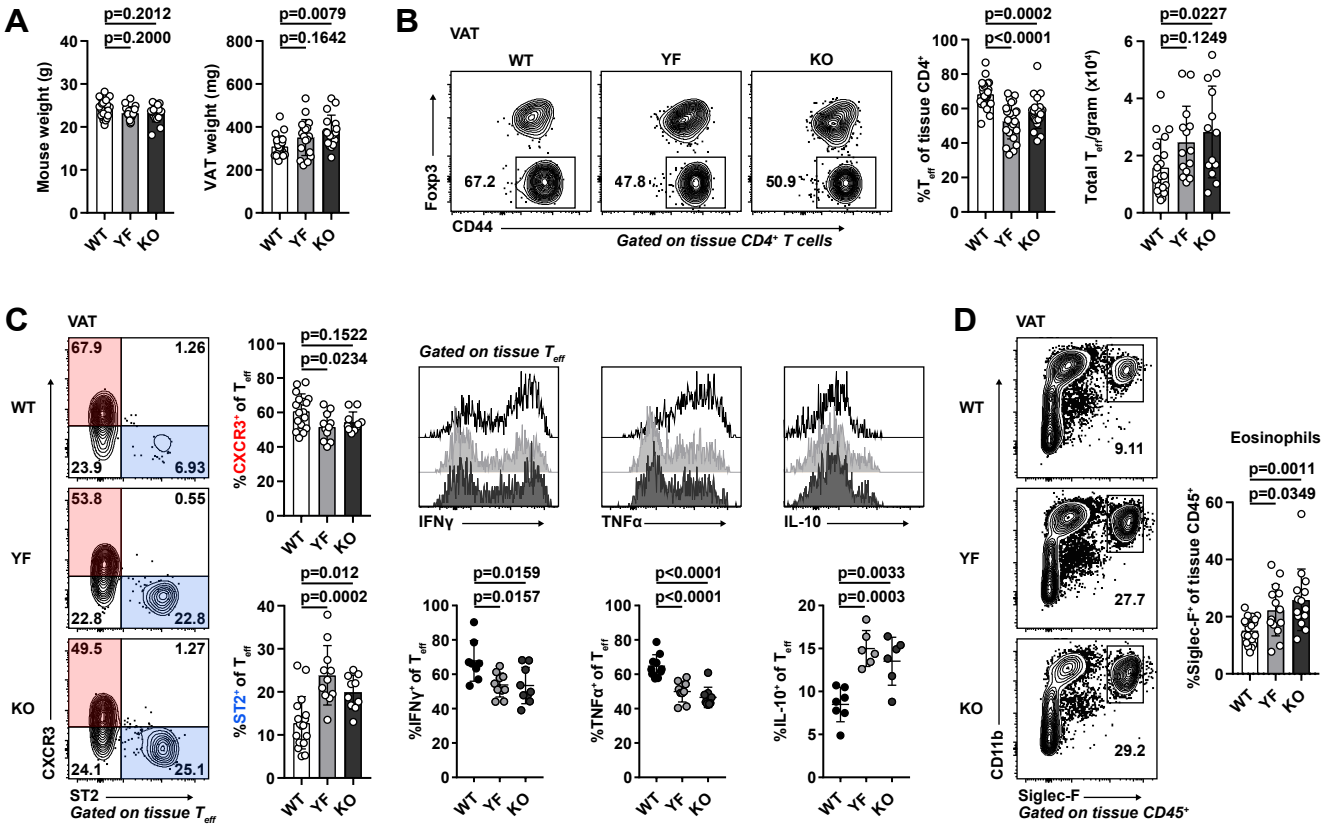


**Figure 4: Reduced expression of inflammatory markers in YF and KO VAT. (A)** Summary of total mouse weight (left panel) and epididymal VAT weight (right panel) in male WT, YF and KO mice. **(B)** VAT-$T_{eff}$ frequencies of tissue-localized TCRβ⁺CD4⁺ cells in WT, YF, and KO mice. Graphical data show $T_{eff}$ frequencies (left graph) and total number $T_{eff}$ per gram of tissue (right graph). **(C)** Representative gating of VAT-$T_{eff}$ on CXCR3 and ST2 expression. Graphs summarize the frequency of WT, YF, and KO VAT-$T_{eff}$ positive for CXCR3 (top) or ST2 (bottom). Representative flow cytometry plots (top panels) and summarized graphical data (bottom panels) of IFNγ, TNFα, and IL-10 expression in $T_{eff}$ from VAT after 4h PMA/I+monensin stimulation *ex vivo*. **(D)** Tissue-localized eosinophil frequencies in VAT. Flow cytometry plots are representative of data from 2 or more independent experiments. Graphical data are compiled from 2 or more independent experiments using mice aged 8-16 weeks, with $n$ = 3-5 mice per group per experiment. Statistical significance was determined using one-way ANOVA with Tukey's post-test. All graphical data are presented as mean values ± SD.

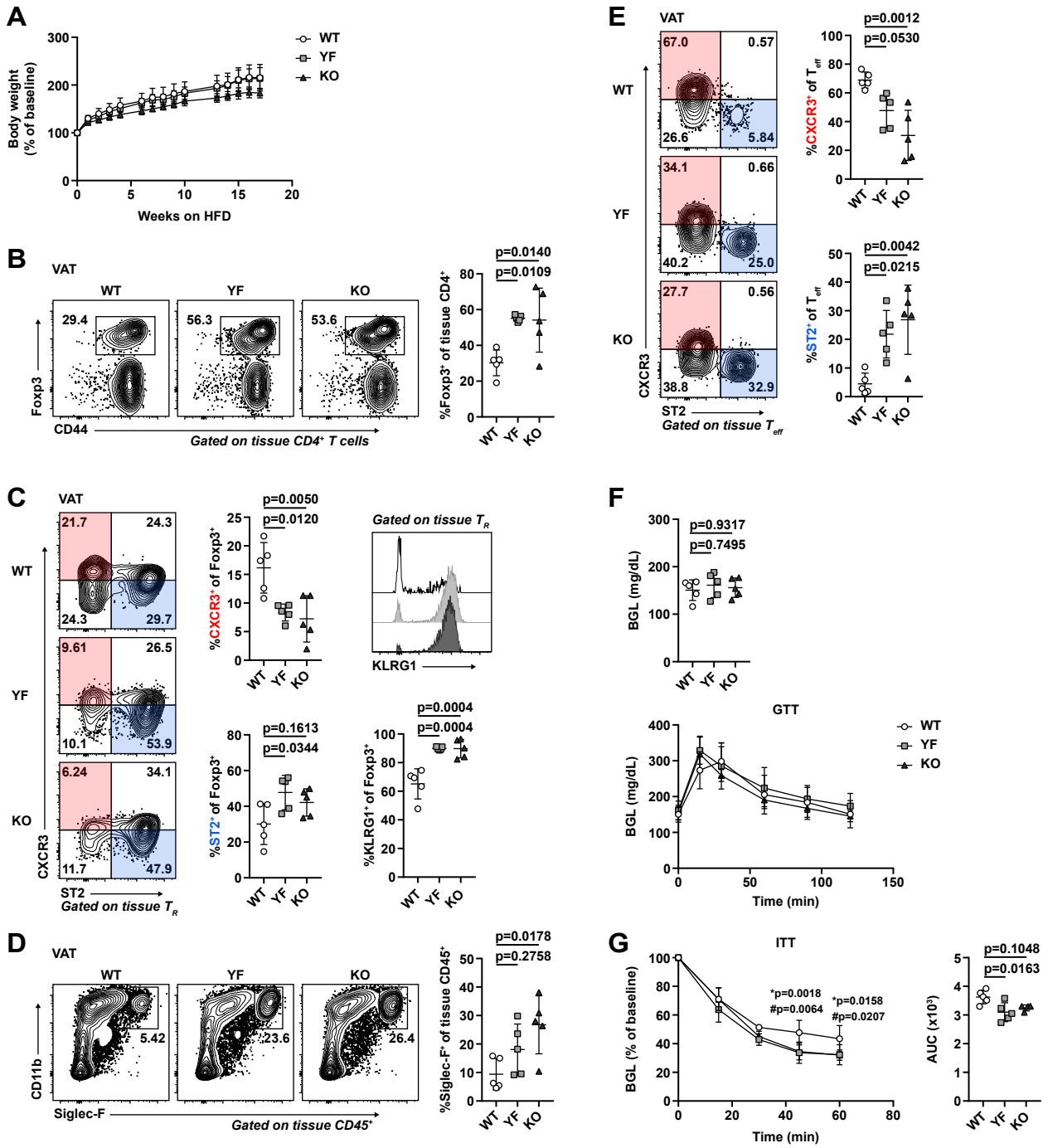


**Figure 5: Mice deficient in ICOS signaling maintain anti-inflammatory immune cell abundance and phenotype in VAT after long-term HFD, correlating with improved insulin sensitivity.** Groups of WT, YF, and KO mice were placed on HFD for 18 wk. **(A)** Fasted body weights taken at indicated timepoints and graphed as percentage of baseline body weight at start of HFD. **(B)** Tissue-localized VAT-$T_R$ frequency at the end of the HFD treatment. **(C)** VAT-$T_R$ phenotypic data as measured by flow cytometry showing expression of CXCR3, ST2, and KLRG1. **(D)** Frequency of tissue-localized eosinophils in VAT. **(E)** Representative gating of VAT-$T_{eff}$ on CXCR3 and ST2 with summarized graphical data. **(F)** Fasting BGL (top) and GTT (bottom) in HFD-fed mice. **(G)** ITT in HFD-fed mice. * indicates significant difference between WT and YF; # indicates significant difference between WT and KO. ITT area under the curve (AUC) was calculated for each individual mouse. Flow cytometry plots are representative of data from 2 experiments. Graphical data are compiled from 2 experiments with *n* = 4-5 mice per group per experiment. For weight **(A)**, GTT, and ITT **(F, G)** graphs, statistical significance was determined using two-way repeated measures ANOVA with Tukey's post-test for multiple comparisons. For fasted BGL **(F)**, ITT AUC **(G)**, and all flow cytometry summary graphs, statistical significance was determined using one-way ANOVA with Tukey's post-test. All graphs are presented as mean values ± SD.

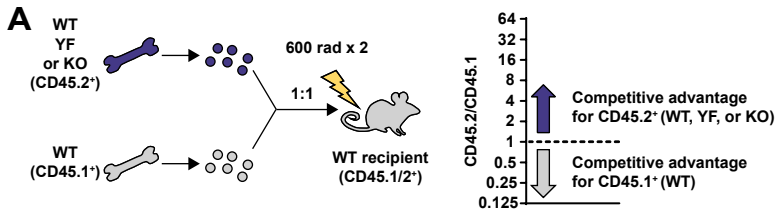
A
WT
YF
or KO
(CD45.2+)
WT
(CD45.1+)
600 rad x 2
1:1
WT recipient
(CD45.1/2+)
CD45.2/CD45.1
Competitive advantage
for CD45.2+ (WT, YF, or KO)
Competitive advantage
for CD45.1+ (WT)

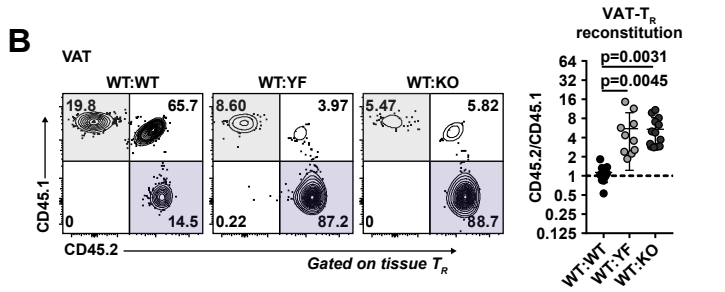
B
VAT
WT:WT
WT:YF
WT:KO
CD45.1
CD45.2
Gated on tissue TR
VAT-TR reconstitution
p=0.0031
p=0.0045
CD45.2/CD45.1
WT:WT
WT:YF
WT:KO

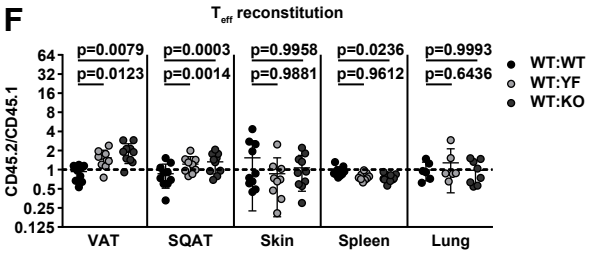
F
Teff reconstitution
p=0.0079
p=0.0123
p=0.0003
p=0.0014
p=0.9958
p=0.9881
p=0.0236
p=0.9612
p=0.9993
p=0.6436
CD45.2/CD45.1
WT:WT
WT:YF
WT:KO
VAT
SQAT
Skin
Spleen
Lung

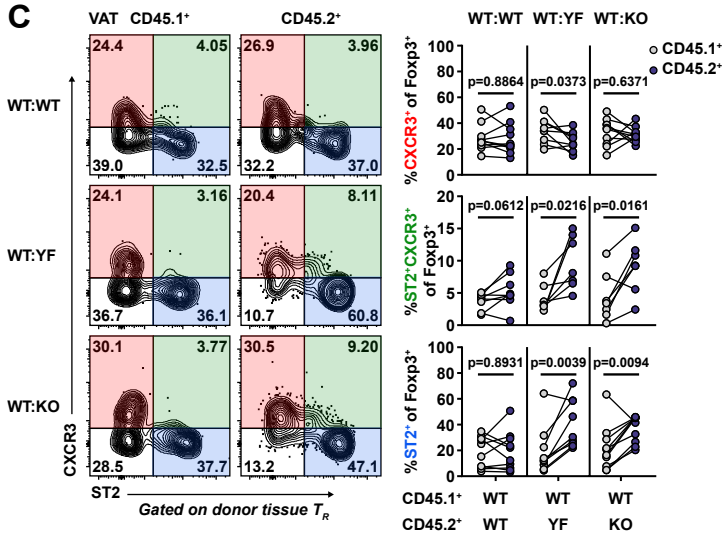
C
VAT
CD45.1+
CD45.2+
WT:WT
WT:YF
WT:KO
CXCR3
ST2
Gated on donor tissue TR
%CXCR3+ of Foxp3+
p=0.8864
p=0.0373
p=0.6371
%ST2+CXCR3+ of Foxp3+
p=0.0612
p=0.0216
p=0.0161
%ST2+ of Foxp3+
p=0.8931
p=0.0039
p=0.0094
CD45.1+ WT WT WT
CD45.2+ WT YF KO

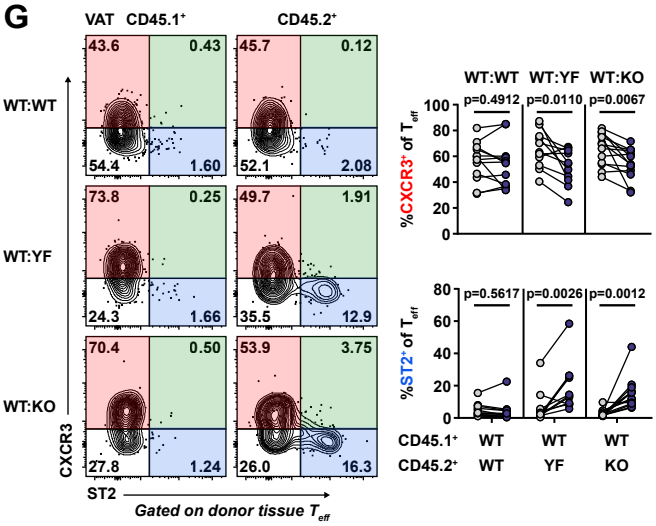
G
VAT
CD45.1+
CD45.2+
WT:WT
WT:YF
WT:KO
CXCR3
ST2
Gated on donor tissue Teff
%CXCR3+ of Teff
p=0.4912
p=0.0110
p=0.0067
%ST2+ of Teff
p=0.5617
p=0.0026
p=0.0012
CD45.1+ WT WT WT
CD45.2+ WT YF KO

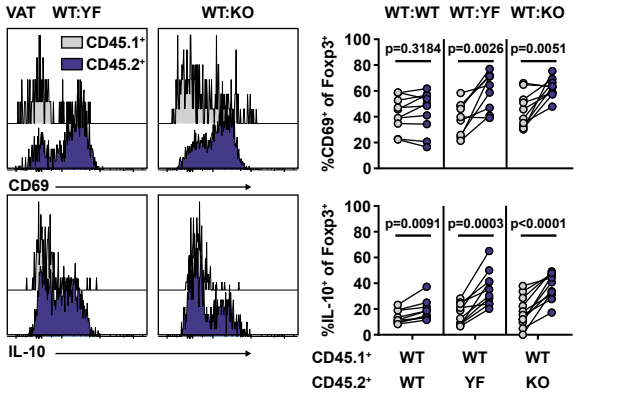
VAT
WT:YF
WT:KO
CD45.1+
CD45.2+
CD69
IL-10
%CD69+ of Foxp3+
p=0.3184
p=0.0026
p=0.0051
%IL-10+ of Foxp3+
p=0.0091
p=0.0003
p<0.0001
CD45.1+ WT WT WT
CD45.2+ WT YF KO

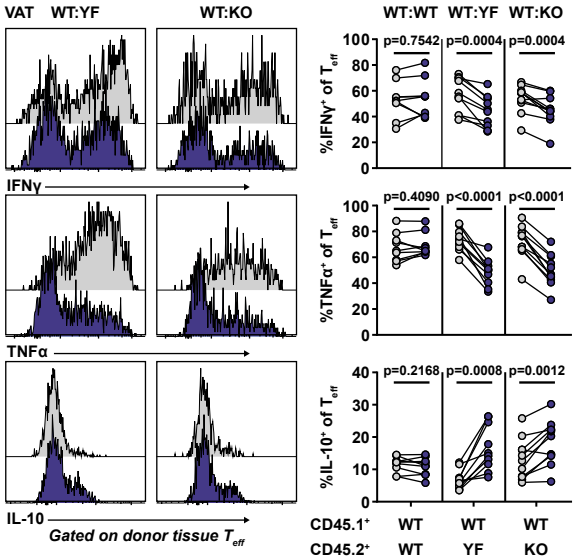
VAT
WT:YF
WT:KO
IFNγ
TNFα
IL-10
Gated on donor tissue Teff
%IFNγ+ of Teff
p=0.7542
p=0.0004
p=0.0004
%TNFα+ of Teff
p=0.4090
p<0.0001
p<0.0001
%IL-10+ of Teff
p=0.2168
p=0.0008
p=0.0012
CD45.1+ WT WT WT
CD45.2+ WT YF KO

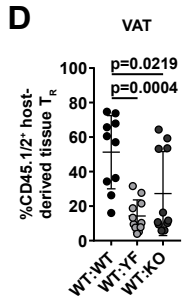
D
VAT
p=0.0219
p=0.0004
%CD45.1/2+ host-derived tissue TR
WT:WT
WT:YF
WT:KO

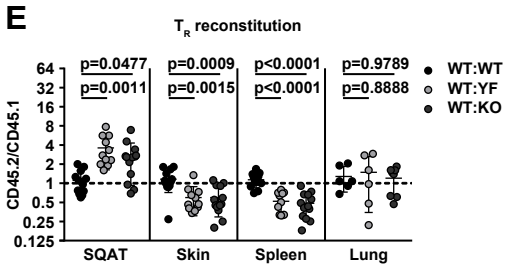
E
TR reconstitution
p=0.0477
p=0.0011
p=0.0009
p=0.0015
p<0.0001
p<0.0001
p=0.9789
p=0.8888
CD45.2/CD45.1
WT:WT
WT:YF
WT:KO
SQAT
Skin
Spleen
Lung

**Figure 6: Cell-intrinsic ICOS signaling limits $T_R$ and $T_{eff}$ abundance and phenotype in VAT. (A)** (Left) Schematic of mixed bone marrow chimera set-up, indicating transfer of CD45.1$^+$ (WT) and CD45.2$^+$ (WT, YF, or KO) hematopoietic cells at a 1:1 ratio into lethally irradiated WT hosts. (Right) Representative graph depicting the method for visualizing donor cell reconstitution as a ratio of CD45.2$^+$:CD45.1$^+$ cells, with the dashed line indicating 1:1 reconstitution. **(B)** Representative gating of CD45.1 vs. CD45.2 expression in chimeric mice on tissue-localized $T_R$ in VAT and graphical analysis of donor $T_R$ reconstitution in VAT. **(C)** (Top) Representative gating on CXCR3- and ST2-expressing CD45.1$^+$ and CD45.2$^+$ donor VAT-$T_R$ in chimeric mice. Line connects points indicating CD45.1$^+$ and CD45.2$^+$ cells within the same chimeric mouse. (Bottom) Histogram and graphical summary of donor VAT-$T_R$ expression of CD69. Histogram and graphical summary of donor VAT-$T_R$ expression of IL-10 after 4hr PMA/I+monensin stimulation *ex vivo*. **(D)** Frequency of endogenous CD45.1/2$^+$ VAT-$T_R$ in chimeric mice. **(E)** Reconstitution of donor $T_R$ in the indicated tissues. **(F)** Summary of donor $T_{eff}$ reconstitution in the indicated tissues. **(G)** (Top) CXCR3 and ST2 expression by gated VAT-$T_{eff}$. (Bottom) Histograms and summary of donor VAT-$T_{eff}$ expression of IFNγ, TNFα, and IL-10 after 4hr PMA/I+monensin stimulation *ex vivo*. Flow cytometry plots are representative of data of 3 independent mixed bone marrow chimera experiments. Graphical data are compiled from 3 independent experiments with $n$ = 3-5 mice per group per experiment. Statistical significance for cell population reconstitution was determined using one-way ANOVA with Tukey's post-test for each tissue analyzed. Data are presented as mean values ± SD. A two-tailed, paired Student's $t$ test was used to assess statistical significance when comparing expression in donor cells within the same chimeric mouse.

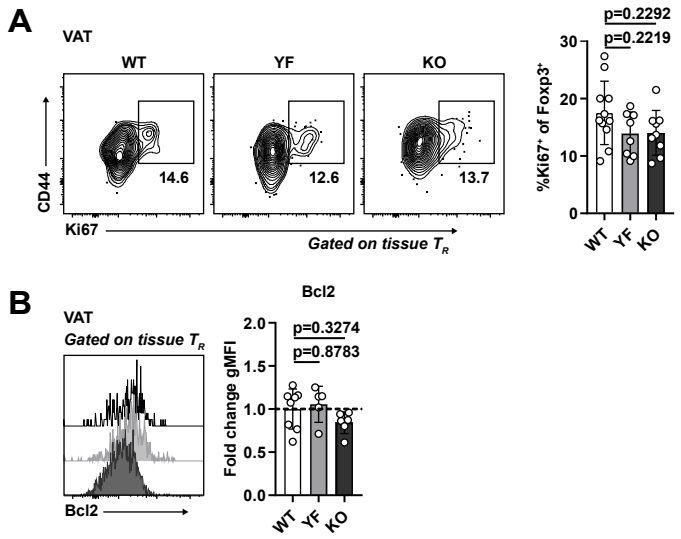


**Figure 7: Increased abundance of YF and KO VAT-$T_R$ is not due to enhanced cellular turnover or survival. (A, B)** Ki67 **(A)** and Bcl2 expression **(B)** in tissue-localized VAT-$T_R$ as measured by flow cytometry directly *ex vivo*. Bcl2 geometric MFI was calculated as fold change compared to average expression in WT $T_R$ for each individual experiment. Flow cytometry plots are representative of data from 2 or more independent experiments. Graphical data are compiled from 2 or more independent experiments using mice aged 8-16 weeks, with *n* = 2-5 mice per group per experiment. Statistical significance was determined using one-way ANOVA with Tukey's post-test. All data are presented as mean values ± SD.

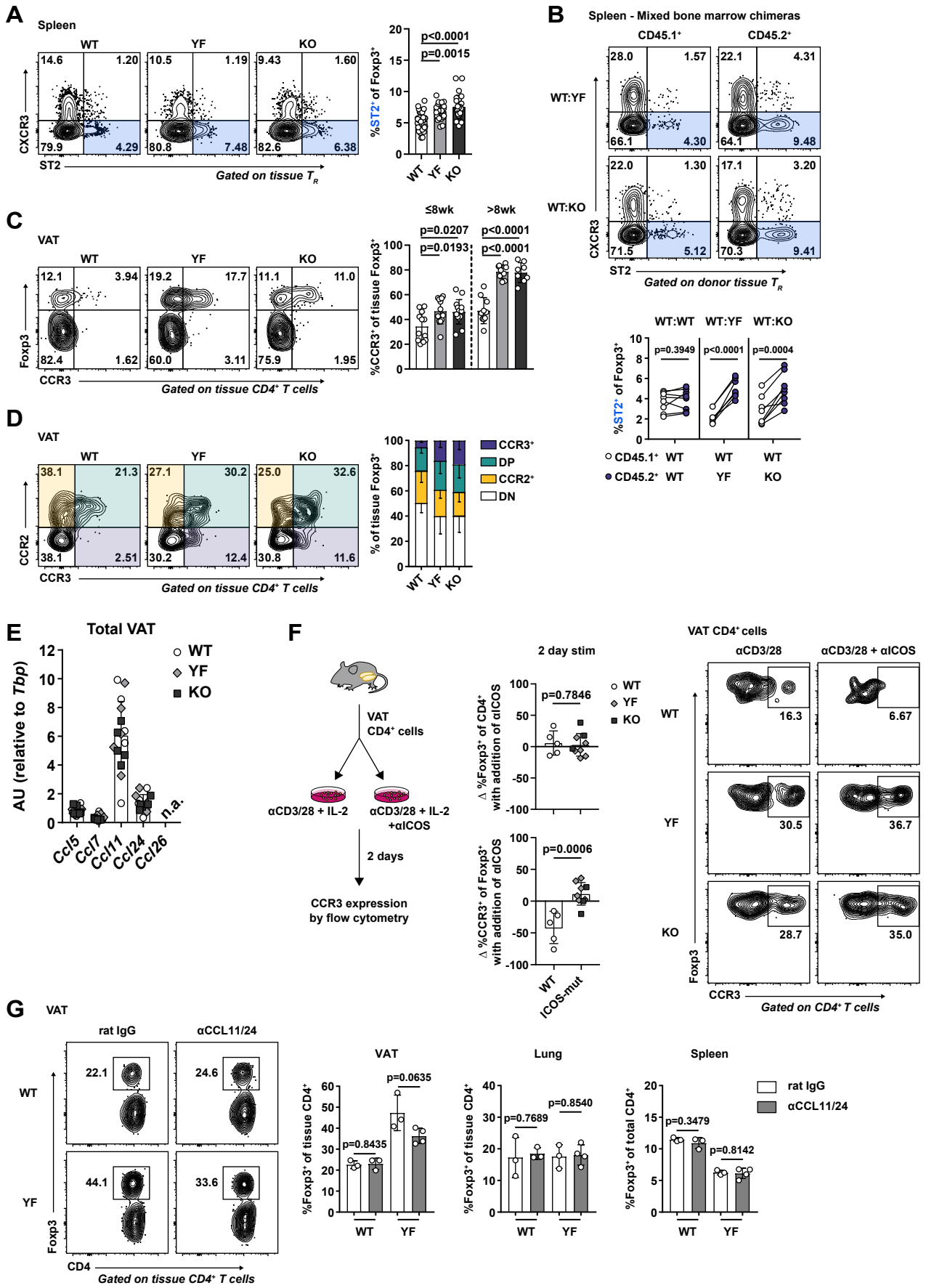
A
Spleen
WT
YF
KO
14.6
1.20
79.9
4.29
10.5
1.19
80.8
7.48
9.43
1.60
82.6
6.38
CXCR3
ST2
Gated on tissue T_R
p<0.0001
p=0.0015
%ST2+ of Foxp3+
B
Spleen - Mixed bone marrow chimeras
CD45.1+
CD45.2+
WT:YF
WT:KO
28.0
1.57
66.1
4.30
22.1
4.31
64.1
9.48
22.0
1.30
71.5
5.12
17.1
3.20
70.3
9.41
Gated on donor tissue T_R
WT:WT
WT:YF
WT:KO
p=0.3949
p<0.0001
p=0.0004
CD45.1+ WT WT WT
CD45.2+ WT YF KO
C
VAT
12.1
3.94
82.4
1.62
19.2
17.7
60.0
3.11
11.1
11.0
75.9
1.95
Foxp3
CCR3
Gated on tissue CD4+ T cells
≤8wk
>8wk
p=0.0207
p=0.0193
p<0.0001
p<0.0001
%CCR3+ of tissue Foxp3+
D
VAT
38.1
21.3
38.1
2.51
27.1
30.2
30.2
12.4
25.0
32.6
30.8
11.6
CCR2
CCR3
Gated on tissue CD4+ T cells
% of tissue Foxp3+
CCR3+
DP
CCR2+
DN
E
Total VAT
AU (relative to Tbp)
WT
YF
KO
Ccl5
Ccl7
Ccl11
Ccl24
Ccl26
n.a.
F
VAT CD4+ cells
αCD3/28 + IL-2
αCD3/28 + IL-2 +αICOS
2 days
CCR3 expression by flow cytometry
2 day stim
p=0.7846
Δ %Foxp3+ of CD4+ with addition of αICOS
p=0.0006
Δ %CCR3+ of Foxp3+ with addition of αICOS
WT
ICOS-mut
VAT CD4+ cells
αCD3/28
αCD3/28 + αICOS
16.3
6.67
30.5
36.7
28.7
35.0
Foxp3
CCR3
Gated on CD4+ T cells
G
VAT
rat IgG
αCCL11/24
22.1
24.6
44.1
33.6
Foxp3
CD4
Gated on tissue CD4+ T cells
VAT
p=0.0635
p=0.8435
%Foxp3+ of tissue CD4+
Lung
p=0.7689
p=0.8540
Spleen
p=0.3479
p=0.8142
%Foxp3+ of total CD4+
WT
YF
rat IgG
αCCL11/24

**Figure 8: Increased VAT-$T_R$ accumulation in the absence of ICOS signaling is associated with elevated CCR3 expression. (A)** ST2 expression in splenic $T_R$ in mice aged 8-16 weeks. **(B)** ST2 expression in CD45.1$^+$ and CD45.2$^+$ donor splenic $T_R$ in WT:YF and WT:KO chimeric mice. Line in graph connects CD45.1$^+$ and CD45.2$^+$ donor splenic $T_R$ within the same chimera. **(C)** Expression of CCR3 in VAT-$T_R$ in mice ≤8 wk and >8 wk of age. **(D)** Expression of CCR2 and CCR3 by VAT-$T_R$. **(E)** Expression of indicated CCR3 ligands in total VAT normalized to *Tbp* as measured by qPCR. **(F)** (Left) Schematic of *in vitro* culture experiments examining the impact of ICOS signaling on CCR3 expression. (Middle) Graphs indicating fold change in $T_R$ frequency of CD4$^+$ cells (top) and %CCR3$^+$ of $T_R$ (bottom) between individual culture samples stimulated with or without αICOS for 2 d. (Right) Representative flow cytometry plots with frequency of CCR3$^+$ $T_R$ after 2 d in specified culture conditions. **(G)** Groups of WT and YF mice were treated intraperitoneally with blocking antibodies against CCL11 and CCL24 every 5 days for 2 wk. (Left) Representative flow cytometry plots indicating VAT-$T_R$ frequency with or without CCL11/24 blockade. Graphs summarize $T_R$ frequencies in indicated tissues after 2 wk. Data in **(G)** are from 1 experiment with $n$ = 3-4 mice per group. For all other experiments, flow cytometry plots are representative of data from 2 or more independent experiments. Graphical data are compiled from 2 or more independent experiments with $n$ = 3-4 per group per experiment. Statistical significance was determined using one-way ANOVA with Tukey's post-test **(A, C)**, two-tailed, paired Student's $t$ test for expression in donor cells within the same chimeric mouse **(B)**, and two-tailed Student's $t$ test **(F, G)**. All data are presented as mean values ± SD.